HHS Public Access

Author manuscript

Mol Cell. Author manuscript; available in PMC 2018 October 19.

Published in final edited form as:

Mol Cell. 2017 October 19; 68(2): 398–413.e6. doi:10.1016/j.molcel.2017.09.016.

The Elongation Factor Spt6 Maintains ESC Pluripotency by Controlling Super-Enhancers and Counteracting Polycomb Proteins

A. Hongjun Wang[1,5], **Aster H. Juan**[1,5], **Kyung Dae Ko**[1], **Pei-Fang Tsai**[1], **Hossein Zare**[1], **Stefania Dell'Orso**[2], and **Vittorio Sartorelli**[1,6,*]

[1]Laboratory of Muscle Stem Cells & Gene Regulation, National Institute of Arthritis, Musculoskeletal and Skin Diseases (NIAMS), National Institutes of Health, Bethesda, MD 20829 USA

[2]High-Throughput Sequencing Unit, National Institute of Arthritis, Musculoskeletal and Skin Diseases (NIAMS), National Institutes of Health, Bethesda, MD 20829 USA

SUMMARY

Spt6 coordinates nucleosome dis- and re-assembly, transcriptional elongation and mRNA processing. Here, we report that depleting Spt6 in ESCs reduced expression of pluripotency factors, increased expression of cell lineage-affiliated developmental regulators, and induced cell morphological and biochemical changes indicative of ESC differentiation. Selective down-regulation of pluripotency factors upon Spt6 depletion may be mechanistically explained by its enrichment at ESC super-enhancers where Spt6 controls histone H3K27 acetylation and methylation, and super-enhancer RNA transcription. In ESCs, Spt6 interacted with the PRC2 core subunit Suz12 and prevented H3K27me3 accumulation at ESC super-enhancers and associated promoters. Biochemical as well as functional experiments revealed that Spt6 could compete for binding of the PRC2 methyltransferase Ezh2 to Suz12 and reduce PRC2 chromatin engagement. Thus, in addition to serving as a histone chaperone and transcription elongation factor, Spt6 counteracts repression by opposing H3K27me3 deposition at critical genomic regulatory regions.

Graphical Abstract

*Correspondence: sartorev@mail.nih.gov.
[5]These authors contributed equally
[6]Lead Contact

SUPPLEMENTAL INFORMATION

Supplemental Information includes seven figures and one table.

AUTHOR CONTRIBUTIONS

A.H.W. and V.S. conceived the project and designed the experiments. A.H.W. and A.H.J. performed the experiments and analyzed the data. P-F.T. helped with subcloning and luciferase assay. K.D.K. and H.Z. performed computational analysis, and S.D. assisted with computational analysis. V.S. supervised the project, analyzed the data and wrote the manuscript with input from A.H.W., A.H.J., and S.D.

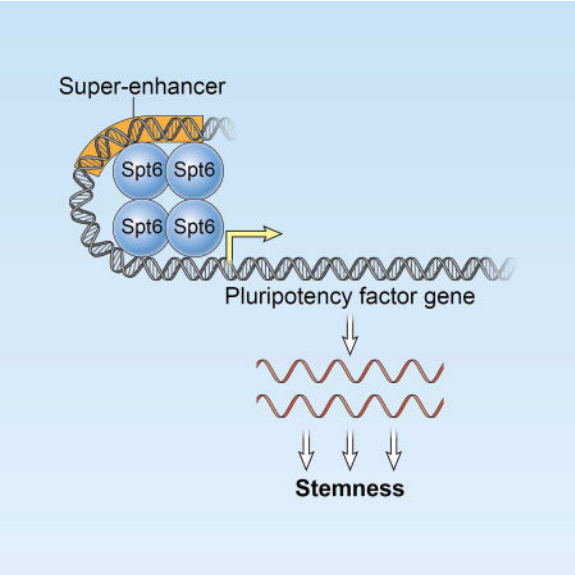

INTRODUCTION

Polycomb Repressive Complex 2 (PRC2) promotes the establishment of repressed chromatin state through trimethylation of lysine 27 of histone H3 (H3K27me3) (Margueron and Reinberg, 2011) and regulates differentiation of mouse embryonic stem cell (ESCs) (Chamberlain et al., 2008) (Shen et al., 2008) (Leeb et al., 2010) (Montgomery et al., 2005) (Pasini et al., 2007) (Cruz-Molina et al., 2017). PRC2 is also required to maintain transcriptional repression of developmental regulators and for self-renewal of human ESCs (Collinson et al., 2016). Even though the individual core PRC2 subunits Ezh2, Suz12, and Eed are highly expressed (Shen et al., 2008), the chromatin of ESCs is partially refractory to H3K27me3. The low percentage of the ESC genome occupied by H3K27me3 (Zhu et al., 2013a) coincides with an hyperdynamic chromatin-protein binding pattern in which a fraction of histones and other chromatin-associated proteins with a short residence time generate a permissive “breathing” chromatin state (Meshorer et al., 2006). PRC2 engagement and H3K27me3 deposition are avoided at ESC regulatory regions of actively transcribed genes, including those for the core pluripotency transcription factors (TFs) Pou5f1 (Oct4), Sox2, and Nanog (henceforth collectively referred to as OSN) (Ng and Surani, 2011) (Young, 2011) (Orkin and Hochedlinger, 2011). OSN bind a set of active enhancers, including their own, implicated in controlling ESC pluripotency (Boyer et al., 2005) (Whyte et al., 2013). However, OSN are also engaged with PRC2 at regulatory regions of repressed or lowly expressed bivalent genes (Azuara et al., 2006) (Bernstein et al., 2006) (Marson et al., 2008) (Young, 2011). Artificial inhibition of transcription or transcriptional elongation results in PRC2 recruitment and H3K27me3 deposition and, conversely, active transcription is mutually exclusive with PRC2 binding (Riising et al., 2014). While active chromatin marks inhibit PRC2 activity (Schmitges et al., 2011), the mechanisms repelling PRC2 binding at transcribed regions remain poorly understood.

Transcriptional elongation is a checkpoint for productive transcription. In ESCs approximately 50% of the genes enriched for H3K4me3 are initially transcribed but do not enter productive elongation (Guenther et al., 2007) (Rahl et al., 2010). Following promoter escape, the transcriptional elongating protein complex needs to overcome the nucleosome barrier (Kwak and Lis, 2013). During this process, the histone chaperones FACT and Spt6 disassemble and reassemble H2A-H2B and H3-H4 dimers, respectively (Bortvin and Winston, 1996) (Belotserkovskaya et al., 2003). Spt6 enhances transcriptional elongation rate (Kaplan et al., 2000) (Endoh et al., 2004) (Ardehali et al., 2009) and interacts with the elongating RNA polymerase II phosphorylated at Ser2 (Ser2P-PolII) (Yoh et al., 2007), a property also required for Spt6 to promote mRNA processing and nuclear export (Yoh et al., 2008). In addition, Spt6 associates with H3K27me3 demethylases KDM6A (UTX) and KDM6B (JMJD3) and H3K36 methyltransferase SETD2 (Wang et al., 2013) (Chen et al., 2012). The Tudor domain of the PRC2-associated Polycomb-like proteins PHF1/PLC1 and PHF19/PLC3 recognize H3K36me3 nucleosomes allowing recruitment and spreading of PRC2 and H3K27me3 into H3K36me3-chromatin regions of ESC (Cai et al., 2013) (Brien et al., 2012). H3K27me3 spreading might be regulated to prevent its intrusion into active chromatin regions.

Here, we report that genome-wide distribution of Spt6 is anti-correlated with PRC2 core subunits Suz12 and Ezh2, and H3K27me3. Spt6 is required to maintain expression of pluripotency TFs in ESCs. Spt6 is enriched at ESC super-enhancers where it controls the balance of H3K27 acetylation and methylation, and enhancer transcription. By specifically interacting with a discrete surface of Suz12, Spt6 competes for Ezh2 binding to Suz12 and curtails chromatin engagement of PRC2 and subsequent H3K27me3. These findings ascribe an additional regulatory role to Spt6 as ESC pluripotency factor and modulator of PRC2 activity.

RESULTS

Spt6 Negatively Correlates with PRC2 and H3K27me3 Occupancy in ESCs

We evaluated the genomic distribution of Spt6 in ESCs by chromatin immunoprecipitation followed by massive parallel sequencing (ChIP-seq). Approximately 56,000 Spt6 peaks were detected with the majority (~61%) of them being located at intragenic regions, ~ 20% at promoters, and ~18% at intergenic regions (Figure S1 and Figure 1A). To refine genomic locations, we intersected ChIP-seq maps for H3K4me3, H3K4me1, H3K27ac, and H3K27me3 (Juan et al., 2016) with Spt6 datasets. Spt6 peaks intersected with ~ 66% (21,657/32,746) H3K4me3^{+}, ~44% (30,697/69,649) H3K4me1^{+}, ~57% (25,535/44,845) H3K27ac^{+}, and ~27% (9,046/33,272) H3K27me3^{+} regions (Figure 1B). More than 95% of active promoters (TSS, H3K4me3^{+}/H3K27ac^{+}) and ~ 90% of bivalent domains (TSS H3K4me3^{+}/H3K27me3^{+}) (Bernstein et al., 2006) (Mikkelsen et al., 2007) were occupied by Spt6. In contrast, Spt6 was detected at only ~ 5% of repressed promoters (TSS H3K4me3^{-}/H3K27me3^{+}) (Figure 1C). Similar percentages of active (~55%) (H3K4me1^{+}/H3K27ac^{+}) and poised (~60%) (H3K4me1^{+}/H3K27me3^{+}) enhancers were occupied by Spt6, respectively (Figure 1C). At transcribed pluripotency factors OSN, Spt6 overlapped with H3K4me3^{+}/H3K27ac^{+} promoter and H3K4me1^{+}/H3K27ac^{+} enhancer regions (Figure 1D).

At *Sox2*, few H3K27me3 islands were present but their position didn't coincide with that of more prominent Spt6 peaks (Figure 1D). Loci for cell lineage-affiliated TFs *Gata2* and *MyoD1* were occupied by H3K27me3 and traces of Spt6 (Figure 1D). To quantitatively determine their respective enrichment, Spt6 or H3K27me3-occupied regions were subdivided in quartiles. Spt6 displayed a graded and inverse occupancy with H3K27me3, with the most enriched Spt6 regions (upper quartile, high Spt6) devoid of H3K27me3 and *vice versa*, the least enriched regions displaying the highest H3K27me3 signal (Figure 1E, left panel). Similarly, enrichment for the PRC2 subunits Suz12 and Ezh2 was anti-correlated with Spt6 (Figure 1E, middle and right panels). Selected ChIP-seq profiles illustrating these findings are shown in Figure S2.

Low H3K27me3 signal at highly enriched Spt6 regions may be related to the ability of Spt6 to associate with and recruit the H3K27 demethylase KDM6A (UTX) (Wang et al., 2013). To investigate this aspect, we performed ChIP-seq for KDM6A which revealed that regions occupied by KMD6A had less H3K27me3 signal, compared to KDM6A-negative regions (Figure 1F). At regions devoid of KDM6A, Spt6 enrichment continued to inversely correlate with H3K27me3 (Figure 1F). Spt6 enrichment was positively associated with gene expression and anti-correlated with H3K27me3 at pluripotency *Zfp42/Rex1* and *Klf2*. The developmental regulator *Pitx2* was repressed, carpeted by H3K27me3 and displayed only traces of Spt6 (Figure 1G). Overall, these findings reveal a genome-wide anti-correlated occupancy of Spt6 and PRC2/H3K27me3.

Spt6 Maintains Expression of ESC Pluripotency Factors

By depleting Spt6 levels, we initially evaluated its role on the regulation of core pluripotency TFs. Compared to control, OSN, Essrb, Klf2, Tcl1 and Prdm14 expression was reduced in Spt6-depleted ESCs (Figure 2 A,B). OSN were also reduced by Spt6 depletion in ESCs cultured in 2i (data not shown), a condition which shields ESCs from differentiation triggers and induces the ground state (Marks et al., 2012).

To obtain a global view on the effects of Spt6 reduction on transcription, we performed RNA-seq (Figure S1). 488 and 895 genes were down- and up-regulated, respectively (Figure 2C, Table S1). Majority of down-regulated genes were occupied by Spt6 (402/488, 82%) whereas only 8% (75/895) of the upregulated genes were bound by Spt6 (Table S1). Downregulated genes displayed ~4-fold more Spt6 signal than upregulated genes (Figure S3A). Gene ontology (GO) analysis identified terms related to nucleosome assembly, negative regulation of cell differentiation and stem cell maintenance among those decreased in Spt6-depleted compared to control ESCs (Figure 2D, upper panel). In addition, other key TFs, including Zfp42, Tfcp2l1, Gbx2, L-Myc (Mycl1) and c-Myc were reduced in Spt6-depleted ESCs (Figure 2E, pluripotency panel and Table S1).

Transcripts upregulated in Spt6-depleted ESC corresponded to terms related to cell adhesion, negative regulation of cell proliferation, and development processes (Figure 2D, lower panel). Expression of mesodermal (ME) and trophoectodermal (TE) developmental regulators was increased (Figure 2E). Some ectodermal transcripts were increased while others, mainly associated with neuroectoderm development (Tubb3, Pax6, Neurod1) were downregulated (Figure 2E). Gene set enrichment analysis (Subramanian et al., 2005)

revealed concordant correlation of the transcriptomic changes observed in Sox2-null (Masui et al., 2007) and Spt6-depleted ESC, further reinforcing a role for Spt6 as a regulator of the ESC pluripotency transcriptional network (Figure S3B,C). Expression of Pitx2 and Pax3 was not increased by Spt6 depletion in ESCs cultured in 2i medium (data not shown), suggesting that upregulation of developmental regulators may be an indirect effect related to premature differentiation, which is prevented when ESCs are kept in the ground state by 2i (Marks et al., 2012).

The morphology of Spt6-depleted colonies was distinct from that of control ESCs. While control ESC colonies were rounded, dome-shaped with well-defined edges, Spt6-depleted ESC colonies appeared to be larger, flattened, with poorly defined margins (Figure 2F, upper panel). Immunoreactivity for the pluripotency marker alkaline phosphatase (AP) was reduced in Spt6-depleted ESC colonies, similar to what observed for differentiated ESCs (Figure 2F, lower panel, Figure S3D). Cre-mediated deletion of floxed-*Spt6* ESCs (obtained from KOMP Repository, UC Davis, USA) resulted in extensive cell death (data not shown), suggesting that a drastic Spt6 reduction is incompatible with cell viability. Thus, Spt6 is required to maintain expression of pluripotency factors in ESCs.

Spt6 is Enriched at and Regulates ESC Super-Enhancers

Super-enhancers (SEs) are clusters of regulatory regions occupied by high levels of the Mediator complex, H3K27 acetylation (ac), RNA polymerase II and other transcriptional coactivators, driving expression of key genes that define cell identity (Whyte et al., 2013) (Hnisz et al., 2013) (Parker et al., 2013) (Qian et al., 2014) (Vahedi et al., 2015). Deletion of specific SE constituents impairs expression of associated pluripotency TF genes (Hnisz et al., 2015). Given the role exerted by Spt6 in regulating expression of pluripotency factors, we compared its distribution with that of the Mediator subunit Med1. Similar to Med1, Spt6 displayed low enrichment at ~8,000 and high enrichment at 231 enhancers corresponding to SEs (Whyte et al., 2013) (Figure 3A). Moreover, Spt6 and H3K27ac were preferentially enriched at SEs (Figure 3A). A direct comparison of tag densities at typical enhancers (TEs) and SEs indicated a significant Spt6 enrichment at the latter (Figure 3B,C). At both *Nanog* and *Pou5f1* (*Oct4*) loci, ChIP-seq profiles showed that, in addition to gene body, Spt6 was enriched at SEs occupied by Med1, and OSN (Figure 3D). Reducing Spt6 levels impaired expression of ESC SE-associated genes (Whyte et al., 2013) (Figure 3E). Spt6 was only slightly enriched at SEs of skeletal muscle C2C12 cells (Figure S4A).

Preferential Spt6 enrichment at SEs prompted us to interrogate H3K27ac in control and Spt6-depleted ESCs. We found that overall H3K27ac protein levels and total H3K27ac ChIP-seq peaks were unaffected by Spt6 depletion (Figure 4A,B). H3K27ac tag density and coverage at TEs were also not overall influenced (Figure 4C,E). In contrast, H3K27ac tag density and coverage were significantly decreased at SEs (Figure 4D,F, Figure S4B). We also analyzed H3K27ac at approximately five hundred (500) enhancer regions with H3K27ac levels comparable to those observed as SEs but not occupied by either pluripotency transcription factors or Mediator complex (Whyte et al., 2013). At these enhancer regions, Spt6 depletion reduced H3K27ac by 2.5-fold less than that observed at

SEs (Figure S4C). Thus, in addition to SEs, Spt6 influences also highly H3K27-acetylated ESC enhancers not occupied by Mediator or pluripotency factors.

H3K27ac at promoter regions of genes associated with TEs was slightly decreased whereas a more profound H3K27ac reduction was observed at promoters associated to SEs (Figure 4G,H). Notably, SE-associated promoters displayed a higher H3K27ac density compared to TE-associated promoters (compare the values on the *x* axis of Figure 4 G and H, respectively). H3K27ac ChIP-seq profiles at TE-associated *Fgfr3* and SE-associated *Klf2* are presented as examples of how Spt6 selectively affects H3K27ac at SEs and SE-associated promoters (Figure 4I,J). Another example of a SE (Dppa3) whose H3K27ac is reduced by Spt6 siRNA is illustrated in Figure S4D. As Spt6 is found in a protein complex containing the H3K36me3 methyltransferase SETD2 (Yoh et al., 2008) involved in transcriptional elongation (Strahl et al., 2002) (Bannister et al., 2005) (Pokholok et al., 2005), we conducted H3K36me3 ChIP-seq in control and Spt6 depleted ESCs. Compared to poised enhancers ($H3K4me1^{+}/H3K27me3^{+}$), SEs displayed increased H3K36me3 occupancy which was reduced by Spt6 depletion (Figure S5A). Consistent with its role in transcriptional elongation, a much higher H3K36me3 enrichment was observed at the body of transcribed genes (compare H3K36me3 Read Coverage scales in Figure S5A and B). Spt6 depletion resulted in markedly reduced H3K36me3 at gene body of downregulated genes (Figure 5B). For instance, H3K36me3 was reduced at both the SE and gene body of the pluripotency factor *Prdm14* (Figure S5C) whose expression is reduced by Spt6 siRNA (Figure 2 and Table S1) and not at the unaffected *HDAC2* gene (Figure S5D). Impaired H3K36me3 at SEs upon Spt6 depletion is consistent with reduced transcription of SE eRNA transcription (see below) and downregulation of selected genes.

H3K27 acetylation and methylation are mutually exclusive and associated with active and inactive enhancers, respectively (Calo and Wysocka, 2013). We wondered whether reduced H3K27ac observed at SEs of Spt6-depleted ESCs would be replaced by H3K27me3. Total H3K27me3 ChIP-seq peaks were comparable (Figure S6A) and H3K27me3 reads were similar at TEs and associated promoters (Figure 5A,C). Instead, H3K27me3 was significantly increased at SEs and associated promoters in Spt6-depleted ESCs (Figure 5B,D, Figure S6B for SEs located at more than 5Kb from TSS). Heatmaps for SEs located at more than 5Kb and 10 Kb from TSS indicated increased H3K27me3 in Spt6-depleted ESC and revealed a differential degree of H3K27me3 at individual regions (Figure S6C). At *Klf2* and *Dppa3* SEs and *Klf2* promoter, H3K27me3 was increased whereas it remained unchanged at the TE of *Fgfr3* (Figure 5E,F, Figure S6D). Since Polycomb group proteins tend to be targeted to CpG islands (CGIs) (Mikkelsen et al., 2007) (Ku et al., 2008), we investigated SE overlap with CGIs in relation to H3K27me3. Approximately 40% of SEs gaining H3K27me3 after Spt6 depletion overlapped CGIs compared to 32% of SEs which did not acquire significant H3K27me3. No difference in CGI overlap was noted for TEs (Figure S6E). To evaluate whether Spt6-occupied ESC SEs acquire H3K27me3 in a physiological setting, we compared H3K27me3 in ESCs, skeletal muscle C2C12 cells and primary cerebellar cells derived from embryonic E 13.5 mice (Mousavi et al., 2012) (Feng et al., 2016). Consistent with reconfiguration of the ESC regulatory network in differentiated cells, H3K27me3 was increased at Spt6-occupied ESC SEs in C2C12 and cerebellar cells (Figure S6F). Such H3K27me3 increase was not observed for TEs assigned to genes

transcriptionally inactive in cerebellar and C2C12 cells (Figure S6G). Increased ESC SEs H3K27me3 in somatic cells was considerably more pronounced that in Spt6-depleted ESCs (Figure S5B,D), a finding not unexpected considering the significant morphological, epigenetic, and transcriptional modifications accompanying cell specification and terminal differentiation (Keller, 2005) (Bibikova et al., 2008) (Young, 2011). Transcription of SEs into RNA (enhancer RNAs, eRNAs) has been observed and related to high levels of RNA polymerase II and transcriptional coactivators (Hnisz et al., 2013) (Mousavi et al., 2013). We found genome-wide levels of SE eRNAs to be reduced in Spt6-depleted ESCs (Figure S6I). Decreased transcription of SE eRNAS generated at Nanog (−45Kb from TSS), Tmem131 (−41Kb from TSS) and Tcf15 (+3Kb from TSS) (Pulakanti et al., 2013) (Ding et al., 2015) was confirmed by quantitative PCR (Figure 5G). As both H3K27ac and eRNA transcription are predictors of enhancer activity (Rada-Iglesias et al., 2011) (Creyghton et al., 2010) (Zhu et al., 2013b) and have been successfully employed to identify functional enhancers in transgenic mouse reporter assays (Wu et al., 2014), our findings indicate that Spt6 regulates the activity of ESC SEs.

Spt6 Interacts with Suz12 and Competes for Ezh2 Binding

Transcriptional inhibition or elongation in ESCs triggers H3K27me3 (Riising et al., 2014). Since we observed that Spt6 depletion resulted in increased H3K27me3 at SEs and associated promoters, we asked whether the negative correlation between PRC2/H3K27me3 and Spt6 distribution might have a biochemical basis. To this end, Flag-tagged Spt6 and HA-tagged Ezh2, Suz12, or Eed were co-expressed in different combinations in 293T cells and cell extracts immunoprecipitated with Flag and probed with HA antibodies. Of the three PRC2 components, Suz12 displayed the strongest interaction with Spt6, while Ezh12 and Eed had slight or no apparent binding, respectively (Figure 6A). Suz12-Spt6 interaction was not affected by RNase treatment, ruling out RNA participation (data not shown). Interaction of endogenous Spt6 and Suz12 proteins from ESC was confirmed in reciprocal immunoprecipitation assay conducted with either Spt6 or Suz12 antibodies in soluble nuclear fractions (Figure 6B). Of note, ESC chromatin-associated Su12 did not interact with Spt6 (Figure S7A), a finding in agreement with the mutually exclusive genome-wide occupancy of Spt6 and PRC2 (Figure 1). To determine whether the Spt6-PRC2 association is direct, baculovirus-produced and purified Spt6 and Suz12, Ezh2, or Eed were tested in immunoprecipitation assay. The results of this assay confirmed that Suz12 robustly and specifically interacts with Spt6, and that such interaction does not require additional proteins (Figure 6C). Spt6 deletions were generated and tested for their ability to interact with Suz12. When expressed in mammalian cells, several non-overlapping Spt6 regions could associate with Suz12 indicating the presence of multiple contact surfaces on Spt6. Two regions of Spt6, one located at the N-terminus (amino acids 1–317) and the other at the C-terminus (amino acids 1299–1726) failed to interact with Suz12 (Figure 6 D,E). Three-dimensional electron microscopy has been recently employed to elucidate the overall architecture of the PRC2 complex, revealing a detailed map of molecular interactions (Ciferri et al., 2012). Within this interaction map, Suz12 makes several contacts with other PRC2 subunits. In particular, two regions of Suz12, one containing the VEFS domain and the other spanning a zinc finger (ZnF) motif make specific contacts with the SANT and SET (enzymatic) domains of Ezh2, respectively (Schmitges et al., 2011) (Ciferri et al., 2012).

Guided by these observations, we generated several GST-Suz12 constructs and obtained bacterially-expressed and purified polypeptides to be tested for interaction with baculovirus-produced Spt6. Of all the regions tested, only a region of mouse Suz12 encompassing amino acids 406–545 [GST-Suz12 (406–545), polypeptide 4] and containing the ZnF motif interacted with Spt6 (Figure 6 F,G). Based on the reported PRC2 architecture, these results suggest that Ezh2 and Spt6 may compete for Suz12 binding. We tested this possibility by incubating constant amounts of recombinant Ezh2 and GST-Suz12 (406–545) polypeptides with increasing amounts of Spt6 and pulling-down using GST beads. With increasing Spt6, less GST-Suz12-associated Ezh2 was recovered, suggesting that Spt6 and Ezh2 compete for Suz12 binding (Figure 6H, Figure S7B). These observations were recapitulated in HEK293T cells by titrating an Spt6-expressing construct in the presence of constant amounts of Suz12 and Ezh2. As observed for recombinant proteins, increasing Spt6 resulted in progressively reduced recovery of Suz12-associated Ezh2 (Figure 6I). These results indicate that Spt6 interacts with Suz12 and competes for Ezh2 binding.

Spt6 Counteracts PRC2 Recruitment and Alleviates Transcriptional Repression

To mechanistically evaluate the functional relevance of the Spt6-Suz12 interaction, we attempted reconstitution experiments with siRNA-resistant full-length or Suz12-binding deficient Spt6 expression vectors in Spt6-depleted ESCs. However, the results of these experiments were not conclusive. Therefore, we turned to a mammalian cell system stably expressing a transgene composed of multimerized Gal4 DNA-binding sites and the thymidine kinase (TK) promoter driving expression of the luciferase gene (Sarma et al., 2008) and a tetracycline-inducible Gal4-Suz12 construct (Figure 7A). Adding tetracycline to the culture medium induced Gal4-Suz12 expression and repressed luciferase activity (Figure 7B,C). ChIP-qPCR performed with a Gal4 antibody and targeted at the Gal4-TK-luc transgene documented increased Gal4-Suz12 recruitment upon tetracycline exposure (Figure 7E). ChIP-qPCR with Ezh2 or H3K27me3 antibodies revealed that Gal4-Suz12 could also recruit endogenous Ezh2 at the Gal4-TK-luc transgene resulting in increased H3K27me3 (Figure 7E). Transient transfection of a Myc-tagged Spt6 construct reduced recruitment of Gal4-Suz12 and Ezh2, and diminished H3K27me3 at the Gal4-TK-luc transgene (Figure 7C,E). Moreover, Gal4-Suz12-induced luciferase repression was partially alleviated by transient transfection of Myc-Spt6 (Figure 7D). To investigate whether the effects of Spt6 on Gal4-TK-luc chromatin and transcription were related to its ability to interact with Suz12, we employed a truncated Spt6 (amino acids 1299–1726) incapable of interacting with Suz12 (Figure 6B). While this truncated version for Spt6 was expressed (Figure 7C), competent for binding to Ser2P-PolII binding (Figure S7C) (Yoh et al., 2007) (Sun et al., 2010), and recruited on the Gal4-TK-luc chromatin (Figure 7E). Nonetheless, it was ineffective in either reducing PRC2 and H3K27me3 or reversing repression induced by Gal4-Suz12 (Figure 7D,E). Altogether, these results are consistent with a role of Spt6 in counteracting chromatin recruitment of PRC2 and H3K27me3.

DISCUSSION

We found that Spt6 depletion in ESCs resulted in decreased expression of pluripotency TFs, reduced accumulation of the pluripotency marker AP protein, increased transcription of cell

lineage-affiliated master TFs as well as morphological changes indicative of early cell differentiation. Transcription of pluripotency TFs, including OSN, was exquisitely sensitive to reduced Spt6 levels which were, on the other hand, sufficient to sustain transcriptional activation of cell lineage-affiliated master TFs. Increased expression of developmental regulators in Spt6 depleted ESCs is likely an indirect effect triggered by entrance into differentiation following loss of ESC pluripotency factors and regulators (Boyer et al., 2005) (Loh et al., 2006) (Masui et al., 2007) (Ding et al., 2015) (Strikoudis et al., 2016). Expression of pluripotency TFs is controlled by SEs, consisting of cluster of enhancers occupied by high levels of the Mediator complex, RNA polymerase II and other transcriptional activators (Parker et al., 2013; Whyte et al., 2013). Spt6 was preferentially enriched at ESC-specific SE and several lines of evidence supported its role in regulating their activity: Spt6 depletion i) affected expression of genes associated with ESC-SEs; ii) decreased H3K27ac and increased H3K27me3 at SEs; and iii) reduced expression of SE-transcribed eRNAs. As in the case of other transcriptional regulators (Loven et al., 2013) (Brown et al., 2014) (Vahedi et al., 2015) (Pelish et al., 2015), Spt6 reduction may selectively affect ESC SE-mediated gene expression by interfering with cooperative and synergistic binding of multiple transcriptional regulators which is more prominent at SEs compared to TEs (Whyte et al., 2013) (Hnisz et al., 2017). Given the interconnectivity of the autoregulatory loop formed by ESC pluripotency TFs with their respective SEs (Hnisz et al., 2013), reduced expression of ESC pluripotency TFs is expected to negatively affect SE activity. However, it seems unlikely that SE inactivation would be the primary consequence of decreased pluripotency TFs levels, as the TFs themselves would have to be first downregulated to exert a negative effect on SEs.

Elongation is a checkpoint in ESC productive transcription (Guenther et al., 2007) (Rahl et al., 2010). The PHD-finger protein Phf5a has been recently shown to regulate ESC pluripotency by stabilizing the elongation Paf1 complex. Ph5a silencing resulted in downregulation of ESC pluripotency markers and upregulation of mesoderm developmental (Strikoudis et al., 2016). A role at ESC enhancers has also been described for Ell3, a member of the Ell family of transcriptional elongation factors and component of the super elongation complex (Miller et al., 2000) (Luo et al., 2012). In ESCs, Ell3 occupies enhancer regions that are poised, active, or inactive and is required for priming of developmental regulators for future activation during differentiation. However, despite being recruited at enhancers of pluripotency TFs OSN, Ell3 was dispensable for their expression (Smith et al., 2011). Thus, distinct elongation factors have different roles at ESC enhancers controlling genes involved in maintaining pluripotency or favoring differentiation.

Suz12 is required for methyltransferase activity, silencing function as well as for PRC2 protein stabilization in somatic as well as in human ESCs (Cao and Zhang, 2004) (Pasini et al., 2004) (Collinson et al., 2016). Our experiments indicate that, in addition to associating with the H3K27 demethylases KDM6A (UTX) (Wang et al., 2013), KDM6B (JMJD3) and KDM7A (KIAA1718), the H3K36 methyltransferase SETD2 (Chen et al., 2012) and Ser2P-PolII (Yoh et al., 2007), Spt6 also interacts with Suz12 in ESCs. Interaction of Spt6 with Eed, another core PRC2 subunit, has been previously reported (Cao et al., 2014), even though we were unable to consistently detect it. The methyltransferase SET domain of Ezh2 makes direct contacts with amino acids located within the ZnF motif of Suz12 and such

interactions are involved in establishing an architecture suitable for PRC2 allosteric regulation (Ciferri et al., 2012). A region spanning the ZnF domain and including additional Suz12 amino acids (amino acids 406–545) directly interacted with Spt6. *In vivo* and *in vitro* titration of Spt6 reduced Suz12-Ezh2 association indicating competition between Spt6 and Ezh2 for Suz12 binding. Consistently, Spt6 inhibits Ezh2 recruitment and H3K27me3 and mitigates transcriptional repression induced by heterologous Gal4-Suz12 in mammalian cells. Nucleoplasmic Spt6-Suz12 interaction may regulate the stoichiometry of Spt6 available for chromatin recruitment and limiting Spt6 would preferentially affect regions particularly vulnerable to decreased Spt6 accretion, such as SEs. Recent work indicates that PRC2 binds by default to non-transcribed CGI genes and that blocking transcription or transcriptional elongation is sufficient to recruit PRC2. Interestingly, preventing transcriptional elongation via Ser2P-PolII inhibition was more efficient in inducing Suz12 recruitment than causing PolII degradation (Riising et al., 2014). While the difference in Suz12 recruitment might be an intrinsic effect of the inhibitors employed, Ser2P-PolII inhibition is expected to hinder Spt6 recruitment which would result in increased PRC2 accretion. An additional mechanism involved in increased H3K27me3 following Spt6 depletion may be related to RNA production. RNA binding has been shown to negatively modulate PRC2 chromatin recruitment and methyltransferase activity (Davidovich et al., 2013) (Cifuentes-Rojas et al., 2014) (Davidovich et al., 2015). In addition to interacting with Suz12, Spt6 may also indirectly counteract PRC2 recruitment and activity at transcribed regions by sustaining RNA production. Recombinant Spt6 did not inhibit *in vitro* methyltransferase activity of preformed PRC2 complex (data not shown), suggesting that Spt6 may prevent PRC2 assembly rather than promoting its disassembly. In *Drosophila melanogaster*, deletion of the Suz12 region involved in Ezh2 and Spt6 interactions results in reduced PRC2 binding to chromatin targets and strong loss of function in genetic rescue tests (Rai et al., 2013). In summary, our findings indicate that, beside behaving as a histone chaperone and transcriptional elongation factor (Kwak and Lis, 2013), Spt6 has the potential of partitioning the genome in transcribed and repressed regions by counteracting formation and recruitment of PRC2 and H3K27me3 at defined regulatory regions.

STAR*METHODS

Detailed methods are provided in the online version of this paper and include the following:

- KEY RESOURCES TABLE
- CONTACT FOR REAGENT AND RESOURCE SHARING
- EXPERIMENTAL MODELS AND SUBJECT DETAILS
  - Cell Lines
  - Bacterial Strains
  - Baculovirus Strains
- METHODS DETAILS
  - Plasmid Construction

- Transfections and RNA Interference
- Alkaline Phosphatase Staining
- Protein Expression and Purification
- Nuclear Extracts, Immunoprecipitation and Immunoblotting
- Quantitative RT-PCR
- RNA Sequencing
- ChIP-Seq and ChIP-qPCR

- QUANTIFICATION AND STATISTICAL ANALYSIS
  - ChIP-seq density analysis
  - Calculation of overlapping regions
  - Heatmap analysis and scatter plots
  - Calculation of read coverage and bean plots
  - Gene ontology analysis
  - Gene Set Enrichment Analysis (GSEA)
- DATA AND SOFTWARE AVAILABILITY

Contact for Reagent and Resource Sharing

Further information and requests for reagents should be directed to Lead Contact Vittorio Sartorelli (sartorev@mail.nih.gov).

Experimental Model and Subject Details

Cell lines—E14 ESCs were grown initially on CF-1 MEF feeder (GlobalStem), passaged feeder-free on gelatin-coated dishes in ES medium (DMEM [GIBCO], 15% HyClone FBS [GE Healthcare], GlutaMAX [GIBCO], MEM nonessential amino acids [GIBCO], sodium pyruvate [GIBCO], leukaemia inhibitory factor [LIF] [Millipore; ESGRO], 0.1 mM β-mercaptoethanol, and antibiotics) or subjected to differentiation by withdrawing LIF for 3 days. Mouse embryonic fibroblasts (MEF) were cultured in DMEM with 10% FBS. HEK293T cells were cultured in DMEM supplemented with 10% FBS. The 293T rex cell line bearing an integrated 5xGal4RE-tk luciferase reporter was kindly provided by Dr. Danny Reinberg. The Gal4-Suz12 construct was stably transfected in the 293T rex luciferase reporter cell line. The tetracycline inducible Gal4-Suz12 293T cell line was grown in medium containing blasticidin (5 μg/ml) to select for the Tet-repressor, G418 (250 μg/ml) to select for the 5xGal4TK-luciferase reporter, and Zeocin (50 μg/ml) to select for the Gal4-Suz12 construct.

Bacterial strains—DH5α, Stbl3, BL21, and DH10α were obtained from Thermo Fisher Scientific, stored at −80°C. DH5α, Stbl3, and DH10α were grown in LB medium at 37°C and used to propagate plasmids. BL21 were grown in LB medium at 30°C and used to express recombinant proteins.

Baculovirus strains—Sf9 insect cells were obtained from Novagen. Sf9 cells were grown in Sf-900 III SFM. These cells were maintained and passaged in adherent or suspension culture at 27°C.

Method Details

Plasmids—Myc-Spt6 vectors have been described (Wang et al., 2013). Flag-tagged Spt6 and deletion mutants were cloned into pCMV-Tag 2B vector (Agilent). HA-Ezh2, HA-Suz12, and HA-Eed plasmids were purchased from Addgene (#24230, #24232, and #24231, respectively). The Suz12 cDNA was subcloned into pcDNA5-FRT-TO vector and fused in frame with the Gal4 DNA binding domain at the N-terminus. Suz12 mutants were cloned into pGEX-4t-1 (GE Healthcare). The Spt6 cDNA was subcloned into pFastBac HT-A vector (Therom Fisher Scientific) for expressing recombinant protein. Baculovirus expression plasmids of Ezh2, Suz12 and Eed were kindly provided by Dr. Danny Reinberg. All plasmids and corresponding sequence information are available upon request.

Transfections and RNA Interference—Transient transfections were performed using Lipofectamine 2000 (Invitrogen). Cells were transfected with control or Spt6 siRNAs with RNAiMAX (Invitrogen) according to manufacturer's protocol.

Alkaline Phosphatase Staining—Alkaline phosphatase staining was performed using the Alkaline Phosphatase Detection Kit (Millipore). Pluripotent E14 ESCs, 3 days-differentiated E14 ESCs or MEF were fixed with 4% paraformaldehyde for 1 minute 48 hours after transfection with control or Spt6 siRNA. Fixed cells were then stained with Naphthol/Fast Red Violet Solution following manufacturer's protocol.

Protein Expression and Purification—Suz12 deletion mutants were cloned into pGEX-4t vector (GE Healthcare) and expressed in *E. coli*. Protein purification was done with Glutathione Sepharose 4B (GE Healthcare) according to manufacturer's protocol. Spt6 were cloned into pFastBac HT (Thermo Fisher Scientific) and expressed in Sf9 cells. Sf9 cells were grown in Grace media supplemented with 10% heat-inactivated FCS. Cells were harvested 72 hr after infection, resuspended in Buffer B containing 20 mM Tris pH 8.0, 10% Glycerol, 300 mM KCl, 5 mM MgCl2 and 0.1% NP40. After sonication and centrifugation, cell lysate was used for purification of recombinant proteins with HisPur Ni-NTA resin (Thermo Scientific) or M2-agarose beads (Sigma). Purified proteins were used for in vitro binding assay.

Nuclear Extracts, Immunoprecipitation and Immunoblotting: For nuclear extracts preparation, ESCs were incubated in 1 ml of hypotonic lysis buffer (20 mM HEPES [pH 7.6], 20% glycerol, 10 mM NaCl, 1.5 mM $MgCl_2$, 0.2 mM EDTA, 0.1% Triton X-100, 25 mM NaF, 1 mM dithiothreitol, protease inhibitors). After 5 min on ice with occasional shaking, the cell lysate was centrifuged for 5 min at 1,300 × g. The nuclear pellet was suspended in 0.2 ml of hypotonic lysis buffer containing 0.5 M NaCl and rotated for 20 min at 4°C. After high-speed centrifugation, the supernatant was collected as the nuclear extract. 500 μg of nuclear extracts were precipitated with normal rabbit IgG (Abcam, ab171870) or anti-Spt6 antibody (Novus, NB100-2582). Bound immunocomplexes were eluted by heat in

LDS sample buffer and subjected to Western analysis with anti-Spt6 or anti-Suz12 antibody (Cell signaling, #3737). For co-IP, 293T cells were cotransfected with plasmids expressing epitope-tagged Spt6 and Suz12, Ezh2 or Eed and harvested with lysis buffer (20mM Tris-HCl [pH 8.0], 10% glycerol, 150mM NaCl, 5mM $MgCl_2$, 0.1% NP-40, protease inhibitors). Whole cell lysate was incubated with anti-flag M2-agarose beads (Sigma). Bound immunocomplexes were eluted by heat in LDS sample buffer and subjected to immunoblotting with anti-HA antibody (Santa Cruz, sc-805). For in vitro binding assay, purified recombinant Spt6 protein was incubated with recombinant Ezh2, Suz12 or Eed proteins, and anti-Spt6 antibody in Buffer B containing 20 mM Tris pH 8.0, 10% Glycerol, 300 mM KCl, 5 mM MgCl2 and 0.1% NP40, then immobilized on protein A sepharose (GE Healthcare). The complexes were washed three times with buffer B–300 mM KCl and once with buffer B– 150 mM KCl and eluted by heat in LDS sample buffer and subjected to immunoblotting with different antibodies against Ezh2, Suz12, Eed or Spt6. For GST pull down assay, the Suz12 fragment 4 was expressed as a fusion with GST in *E. coli*, immobilized on Gutathione Sephaseose 4B (GE Healthcare) beads and incubated with purified recombinant Ezh2 protein and different amount of Spt6 protein. The bound complexes were eluted by heat in LDS sample buffer and subjected to immunoblotting with different antibodies against Ezh2, Spt6 or GST. The intensity of the band was measured by ImageJ (NIH).

Quantitative RT-PCR—Total RNA was extracted using TRIzol Reagent (Invitrogen) according to manufacturer's protocol. cDNA was synthesized with High Capacity cDNA Reverse Transcription Kit (Applied Biosystems) containing random primers and using 500 ng of extracted RNA per sample. Reverse transcribed cDNA was diluted 1:10 and SYBR green real-time PCR was performed on the Applied Biosystems StepOne Plus Real-Time PCR system. mRNA levels were normalized to *GAPDH*.

RNA-sequencing—Total RNA was prepared by using TRIzol (Invitrogen). Two-hundred nanograms to 1 μg of total RNA was subsequently used to prepare RNA-seq libraries by using TruSeq SR RNA sample prep kit (FC-122–1001, Illumina) or by a combination of NEBNext RNA library prep kit (New England BioLabs) and Ovation SP Ultralow DR Multiplex system (Nugen) by following the manufacturer's protocol. The libraries were sequenced for 50 cycles (single read) with HiSeq 2000 or HiSeq 2500 (Illumina).

ChIP-qPCR and ChIP followed by sequencing (ChIP-Seq)—Chromatin immunoprecipitation was performed as previously described (Mousavi et al., 2012) using antibodies against Spt6 (Novus), KDM6A (Sigma), Suz12 (Cell signaling), Ezh2 (Cell signaling), H3K27me3 (Cell signaling), H3K27ac (Abcam), H3K36me3 (Abcam), Gal4 (Millipore), Flag (Sigma, F3165), Myc (Sigma), IgG (Abcam). Real-time PCR was performed with a SyberGreen MasterMix (Applied Biosystems) on a StepOnePlus realtime PCR system (Applied Biosystems). Oligonucleotides employed in ChIP-qPCR for the Gal4-TK-luc system are reported in Supplemental Information. For sequencing, the DNA fragments were blunt-end ligated to the Illumina adaptors and amplified via Mondrian SP Workstation system (NuGEN). Libraries were sequenced for 50 cycles on Illumina HiSeq 2000, HiSeq 2500 or HiSeq3000. Mock DNA (input DNA) was used against the matched

sample data to call enriched regions and control for the false-positive detection rate (FDR). ChIP-seq data of H3K27me3, H3K27ac, H3K4me1, H3K4me3 in mouse ESCs were published in (Juan et al., 2016). ChIP-seq data of Med1, Oct4, Sox2, and Nanog in mouse ESC (Whyte et al., 2013) were downloaded and processed with the same settings.

Quantification and Statistical Analysis

ChIP-seq reads were demultiplexed by CASAVA pipeline (Illumina) and aligned to the mouse reference genome (mm9) using Bowtie with default parameters, except for setting '-l/--seedlen' to 32 and '-m' to 20 (Langmead et al., 2009). PCR duplicate reads were removed and enriched regions for histone modification were called at the FDR level of 5% using SICER (Zang et al., 2009) with window and gap sizes set to 200 bp and 600 bp, respectively. ChIP-seq profiles around TSS sites were generated using custom-made code in Matlab by directly mapping the reads into 100 bp overlapping bins, with sliding width of 50 bp, and normalized to total reads. Bedtools (Quinlan and Hall, 2010) was used for peak annotation and overlapping enriched regions and Homer (Heinz et al., 2010) was used for peak annotation. To compare genomic tracks between WT and Spt6KO, the wig files of samples are generated by MAC2 with broad peak calling option (Zhang et al., 2008). Similarly, RNA-seq reads were generated on the Illumina platform and de-multiplexed by CASAVA. Reads were mapped to the mouse reference genome (mm9) by Tophat2 (Kim et al., 2013) with default parameters. Cufflinks/Cuffdiff (Trapnell et al., 2013) was used for the assignment of reads to transcripts and FPKM (RPKM) values were generated by applying multi-read correction and geometric normalization.

ChIP-Seq Density Analysis—ChIP-seq read densities plots were generated as described in (Shen et al., 2014). Briefly, ChIP-seq reads were extended to the expected DNA fragment length from user input, and the coverage vectors were calculated from their extended reads. Then, the coverage vectors were normalized against the corresponding library size to generate the Reads Per Million mapped reads (RPM) values. Spt6, H3K27 acetylation and H3K27me3 at typical and super-enhancers (Whyte et al., 2013) were determined by first quantifying tag levels ±2 kb from the summits of the peak regions using Homer (Heinz et al., 2010) through normalization. Then, Spt6, H3K27 acetylation, and H3K27me3 were compared based on distances through Boxplot and Beanplot with a statistical test (student's t-test) after calculating the averaged tag levels in identified ChIP-seq enriched regions.

Calculation of overlapping regions—The distribution of Spt6 at intergenic, intragenic and promoter (±1Kb) regions from the summits of the regions were identified by Bedtools. To evaluate the distributions of Spt6 at H3K4me1, H3K27me3, and H3K27 acetylated regions, the number of overlapping regions between Spt6 and H3K4me1, H3K27me3, and H3K27 acetylated regions was calculated using Bedtools with default parameters (Quinlan and Hall, 2010).

Heatmap analysis and scattering plot: Cufflinks, cummeRbund, and pheatmap in R packages were employed to generate heatmaps of RNA-seq data. After FPKMs were calculated using Cufflink, matrices were generated using cummRbund. The fold changes were normalized after calculating fold changes of genes between control and Spt6 siRNA

ESCs samples. Using the pheatmap and scattering plot packages in R, heatmaps and scattering plot related to RNA-expression between control and Spt6 siRNA ESCs were subsequently generated. Genes differentially expressed between WT and Spt6-depleted ESCs were determined according to fold change (FC) more than 1.5-fold (up-regulated) or less than 1.5-fold (down-regulated).

Calculation of read coverage and Bean plot—The read coverages of all samples were calculated by Homer (Heinz et al., 2010). After calculation, the coverages among samples were compared using beanplots in R packages. To test quantitative significances among samples, student t-test was used among samples.

Gene ontology analysis—To determine GO terms enriched in down- and up-regulated genes between control and Spt6 siRNA ESCs, we used the DAVID web-tool with their down and up-regulated genes (Huang da et al., 2009). Molecular Function terms in Gene Ontology were analyzed, and the most significant Gene Ontology terms were reported with their respective p-values.

Gene Set Enrichment Analysis (GSEA)—GSEA (http://www.broadinstitute.org/gsea) was employed to evaluate whether the gene sets of interest were significantly enriched in Spt6 siRNA versus control si RNA RNA-seq data. The Spt6 siRNA gene sets were compared to down- and up-regulated genes in Sox2- null ESCs (Masui et al., 2007).

Data and Software Availability

All software used in this study and the accession number for the ChIP-seq and RNA-seq data are listed in the Key Resources Table.

Supplementary Material

Refer to Web version on PubMed Central for supplementary material.

Acknowledgments

We thank Gustavo Gutierrez-Cruz (NIAMS Sequencing Facility) for libraries preparation and sequencing; Elif Eren (Laboratory of Structural Biology Research, NIAMS) for help with interpreting the Spt6/Suz12 interaction results, and Danny Reinberg (New York University) for providing reagents. This work was supported by the Intramural Research Program of NIAMS at the NIH.

References

Ardehali MB, Yao J, Adelman K, Fuda NJ, Petesch SJ, Webb WW, Lis JT. Spt6 enhances the elongation rate of RNA polymerase II in vivo. The EMBO journal. 2009; 28:1067–1077. [PubMed: 19279664]

Azuara V, Perry P, Sauer S, Spivakov M, Jorgensen HF, John RM, Gouti M, Casanova M, Warnes G, Merkenschlager M, et al. Chromatin signatures of pluripotent cell lines. Nature cell biology. 2006; 8:532–538. [PubMed: 16570078]

Bannister AJ, Schneider R, Myers FA, Thorne AW, Crane-Robinson C, Kouzarides T. Spatial distribution of di- and tri-methyl lysine 36 of histone H3 at active genes. Journal of Biological Chemistry. 2005; 280:17732–17736. [PubMed: 15760899]

Belotserkovskaya R, Oh S, Bondarenko VA, Orphanides G, Studitsky VM, Reinberg D. FACT facilitates transcription-dependent nucleosome alteration. Science. 2003; 301:1090–1093. [PubMed: 12934006]

Bernstein BE, Mikkelsen TS, Xie X, Kamal M, Huebert DJ, Cuff J, Fry B, Meissner A, Wernig M, Plath K, et al. A bivalent chromatin structure marks key developmental genes in embryonic stem cells. Cell. 2006; 125:315–326. [PubMed: 16630819]

Bibikova M, Laurent LC, Ren B, Loring JF, Fan JB. Unraveling epigenetic regulation in embryonic stem cells. Cell stem cell. 2008; 2:123–134. [PubMed: 18371433]

Birve A, Sengupta AK, Beuchle D, Larsson J, Kennison JA, Rasmuson-Lestander A, Muller J. Su(z)12, a novel Drosophila Polycomb group gene that is conserved in vertebrates and plants. Development. 2001; 128:3371–3379. [PubMed: 11546753]

Bortvin A, Winston F. Evidence that Spt6p controls chromatin structure by a direct interaction with histones. Science. 1996; 272:1473–1476. [PubMed: 8633238]

Boyer LA, Lee TI, Cole MF, Johnstone SE, Levine SS, Zucker JP, Guenther MG, Kumar RM, Murray HL, Jenner RG, et al. Core transcriptional regulatory circuitry in human embryonic stem cells. Cell. 2005; 122:947–956. [PubMed: 16153702]

Brien GL, Gambero G, O'Connell DJ, Jerman E, Turner SA, Egan CM, Dunne EJ, Jurgens MC, Wynne K, Piao L, et al. Polycomb PHF19 binds H3K36me3 and recruits PRC2 and demethylase NO66 to embryonic stem cell genes during differentiation. Nature structural & molecular biology. 2012; 19:1273–1281.

Brown JD, Lin CY, Duan Q, Griffin G, Federation AJ, Paranal RM, Bair S, Newton G, Lichtman AH, Kung AL, et al. NF-kappaB directs dynamic super enhancer formation in inflammation and atherogenesis. Molecular cell. 2014; 56:219–231. [PubMed: 25263595]

Cai L, Rothbart SB, Lu R, Xu B, Chen WY, Tripathy A, Rockowitz S, Zheng D, Patel DJ, Allis CD, et al. An H3K36 methylation-engaging Tudor motif of polycomb-like proteins mediates PRC2 complex targeting. Molecular cell. 2013; 49:571–582. [PubMed: 23273982]

Calo E, Wysocka J. Modification of enhancer chromatin: what, how, and why? Molecular cell. 2013; 49:825–837. [PubMed: 23473601]

Cao Q, Wang X, Zhao M, Yang R, Malik R, Qiao Y, Poliakov A, Yocum AK, Li Y, Chen W, et al. The central role of EED in the orchestration of polycomb group complexes. Nature communications. 2014; 5:3127.

Cao R, Zhang Y. SUZ12 Is Required for Both the Histone Methyltransferase Activity and the Silencing Function of the EED-EZH2 Complex. Molecular cell. 2004; 15:57–67. [PubMed: 15225548]

Chamberlain SJ, Yee D, Magnuson T. Polycomb repressive complex 2 is dispensable for maintenance of embryonic stem cell pluripotency. Stem Cells. 2008; 26:1496–1505. [PubMed: 18403752]

Chen S, Ma J, Wu F, Xiong LJ, Ma H, Xu W, Lv R, Li X, Villen J, Gygi SP, et al. The histone H3 Lys 27 demethylase JMJD3 regulates gene expression by impacting transcriptional elongation. Genes & development. 2012; 26:1364–1375. [PubMed: 22713873]

Ciferri C, Lander GC, Maiolica A, Herzog F, Aebersold R, Nogales E. Molecular architecture of human polycomb repressive complex 2. eLife. 2012; 1:e00005. [PubMed: 23110252]

Cifuentes-Rojas C, Hernandez AJ, Sarma K, Lee JT. Regulatory interactions between RNA and polycomb repressive complex 2. Molecular cell. 2014; 55:171–185. [PubMed: 24882207]

Collinson A, Collier AJ, Morgan NP, Sienerth AR, Chandra T, Andrews S, Rugg-Gunn PJ. Deletion of the Polycomb-Group Protein EZH2 Leads to Compromised Self-Renewal and Differentiation Defects in Human Embryonic Stem Cells. Cell reports. 2016; 17:2700–2714. [PubMed: 27926872]

Creyghton MP, Cheng AW, Welstead GG, Kooistra T, Carey BW, Steine EJ, Hanna J, Lodato MA, Frampton GM, Sharp PA, et al. From the Cover: Histone H3K27ac separates active from poised enhancers and predicts developmental state. Proceedings of the National Academy of Sciences of the United States of America. 2010; 107:21931–21936. [PubMed: 21106759]

Cruz-Molina S, Respuela P, Tebartz C, Kolovos P, Nikolic M, Fueyo R, van Ijcken WF, Grosveld F, Frommolt P, Bazzi H, et al. PRC2 Facilitates the Regulatory Topology Required for Poised Enhancer Function during Pluripotent Stem Cell Differentiation. Cell stem cell. 2017

Davidovich C, Wang X, Cifuentes-Rojas C, Goodrich KJ, Gooding AR, Lee JT, Cech TR. Toward a consensus on the binding specificity and promiscuity of PRC2 for RNA. Molecular cell. 2015; 57:552–558. [PubMed: 25601759]

Davidovich C, Zheng L, Goodrich KJ, Cech TR. Promiscuous RNA binding by Polycomb repressive complex 2. Nature structural & molecular biology. 2013

Ding J, Huang X, Shao N, Zhou H, Lee DF, Faiola F, Fidalgo M, Guallar D, Saunders A, Shliaha PV, et al. Tex10 Coordinates Epigenetic Control of Super-Enhancer Activity in Pluripotency and Reprogramming. Cell stem cell. 2015; 16:653–668. [PubMed: 25936917]

Endoh M, Zhu W, Hasegawa J, Watanabe H, Kim DK, Aida M, Inukai N, Narita T, Yamada T, Furuya A, et al. Human Spt6 stimulates transcription elongation by RNA polymerase II in vitro. Mol Cell Biol. 2004; 24:3324–3336. [PubMed: 15060154]

Feng X, Juan AH, Wang HA, Ko KD, Zare H, Sartorelli V. Polycomb Ezh2 controls the fate of GABAergic neurons in the embryonic cerebellum. Development. 2016; 143:1971–1980. [PubMed: 27068104]

Guenther MG, Levine SS, Boyer LA, Jaenisch R, Young RA. A chromatin landmark and transcription initiation at most promoters in human cells. Cell. 2007; 130:77–88. [PubMed: 17632057]

Heinz S, Benner C, Spann N, Bertolino E, Lin YC, Laslo P, Cheng JX, Murre C, Singh H, Glass CK. Simple combinations of lineage-determining transcription factors prime cis-regulatory elements required for macrophage and B cell identities. Molecular cell. 2010; 38:576–589. [PubMed: 20513432]

Hnisz D, Abraham BJ, Lee TI, Lau A, Saint-Andre V, Sigova AA, Hoke HA, Young RA. Super-enhancers in the control of cell identity and disease. Cell. 2013; 155:934–947. [PubMed: 24119843]

Hnisz D, Schuijers J, Lin CY, Weintraub AS, Abraham BJ, Lee TI, Bradner JE, Young RA. Convergence of developmental and oncogenic signaling pathways at transcriptional super-enhancers. Molecular cell. 2015; 58:362–370. [PubMed: 25801169]

Hnisz D, Shrinivas K, Young RA, Chakraborty AK, Sharp PA. A Phase Separation Model for Transcriptional Control. Cell. 2017; 169:13–23. [PubMed: 28340338]

Huang da W, Sherman BT, Lempicki RA. Systematic and integrative analysis of large gene lists using DAVID bioinformatics resources. Nat Protoc. 2009; 4:44–57. [PubMed: 19131956]

Juan AH, Wang S, Ko KD, Zare H, Tsai PF, Feng X, Vivanco KO, Ascoli AM, Gutierrez-Cruz G, Krebs J, et al. Roles of H3K27me2 and H3K27me3 Examined during Fate Specification of Embryonic Stem Cells. Cell reports. 2016; 17:1369–1382. [PubMed: 27783950]

Kaplan CD, Morris JR, Wu C, Winston F. Spt5 and spt6 are associated with active transcription and have characteristics of general elongation factors in D. melanogaster. Genes & development. 2000; 14:2623–2634. [PubMed: 11040216]

Keller G. Embryonic stem cell differentiation: emergence of a new era in biology and medicine. Genes & development. 2005; 19:1129–1155. [PubMed: 15905405]

Kim D, Pertea G, Trapnell C, Pimentel H, Kelley R, Salzberg SL. TopHat2: accurate alignment of transcriptomes in the presence of insertions, deletions and gene fusions. Genome biology. 2013; 14:R36. [PubMed: 23618408]

Ku M, Koche RP, Rheinbay E, Mendenhall EM, Endoh M, Mikkelsen TS, Presser A, Nusbaum C, Xie X, Chi AS, et al. Genomewide analysis of PRC1 and PRC2 occupancy identifies two classes of bivalent domains. PLoS genetics. 2008; 4:e1000242. [PubMed: 18974828]

Kwak H, Lis JT. Control of transcriptional elongation. Annu Rev Genet. 2013; 47:483–508. [PubMed: 24050178]

Langmead B, Trapnell C, Pop M, Salzberg SL. Ultrafast and memory-efficient alignment of short DNA sequences to the human genome. Genome biology. 2009; 10:R25. [PubMed: 19261174]

Leeb M, Pasini D, Novatchkova M, Jaritz M, Helin K, Wutz A. Polycomb complexes act redundantly to repress genomic repeats and genes. Genes & development. 2010; 24:265–276. [PubMed: 20123906]

Loh YH, Wu Q, Chew JL, Vega VB, Zhang W, Chen X, Bourque G, George J, Leong B, Liu J, et al. The Oct4 and Nanog transcription network regulates pluripotency in mouse embryonic stem cells. Nature genetics. 2006; 38:431–440. [PubMed: 16518401]

Loven J, Hoke HA, Lin CY, Lau A, Orlando DA, Vakoc CR, Bradner JE, Lee TI, Young RA. Selective inhibition of tumor oncogenes by disruption of super-enhancers. Cell. 2013; 153:320–334. [PubMed: 23582323]

Luo Z, Lin C, Shilatifard A. The super elongation complex (SEC) family in transcriptional control. Nat Rev Mol Cell Biol. 2012; 13:543–547. [PubMed: 22895430]

Margueron R, Reinberg D. The Polycomb complex PRC2 and its mark in life. Nature. 2011; 469:343–349. [PubMed: 21248841]

Marks H, Kalkan T, Menafra R, Denissov S, Jones K, Hofemeister H, Nichols J, Kranz A, Stewart AF, Smith A, et al. The transcriptional and epigenomic foundations of ground state pluripotency. Cell. 2012; 149:590–604. [PubMed: 22541430]

Marson A, Levine SS, Cole MF, Frampton GM, Brambrink T, Johnstone S, Guenther MG, Johnston WK, Wernig M, Newman J, et al. Connecting microRNA genes to the core transcriptional regulatory circuitry of embryonic stem cells. Cell. 2008; 134:521–533. [PubMed: 18692474]

Masui S, Nakatake Y, Toyooka Y, Shimosato D, Yagi R, Takahashi K, Okochi H, Okuda A, Matoba R, Sharov AA, et al. Pluripotency governed by Sox2 via regulation of Oct3/4 expression in mouse embryonic stem cells. Nature cell biology. 2007; 9:625–U626. [PubMed: 17515932]

Meshorer E, Yellajoshula D, George E, Scambler PJ, Brown DT, Misteli T. Hyperdynamic plasticity of chromatin proteins in pluripotent embryonic stem cells. Developmental cell. 2006; 10:105–116. [PubMed: 16399082]

Mikkelsen TS, Ku M, Jaffe DB, Issac B, Lieberman E, Giannoukos G, Alvarez P, Brockman W, Kim TK, Koche RP, et al. Genome-wide maps of chromatin state in pluripotent and lineage-committed cells. Nature. 2007; 448:553–560. [PubMed: 17603471]

Miller T, Williams K, Johnstone RW, Shilatifard A. Identification, cloning, expression, and biochemical characterization of the testis-specific RNA polymerase II elongation factor ELL3. The Journal of biological chemistry. 2000; 275:32052–32056. [PubMed: 10882741]

Montgomery ND, Yee D, Chen A, Kalantry S, Chamberlain SJ, Otte AP, Magnuson T. The murine polycomb group protein Eed is required for global histone H3 lysine-27 methylation. Curr Biol. 2005; 15:942–947. [PubMed: 15916951]

Mousavi K, Zare H, Dell'orso S, Grontved L, Gutierrez-Cruz G, Derfoul A, Hager GL, Sartorelli V. eRNAs promote transcription by establishing chromatin accessibility at defined genomic loci. Molecular cell. 2013; 51:606–617. [PubMed: 23993744]

Mousavi K, Zare H, Wang AH, Sartorelli V. Polycomb protein Ezh1 promotes RNA polymerase II elongation. Molecular cell. 2012; 45:255–262. [PubMed: 22196887]

Ng HH, Surani MA. The transcriptional and signalling networks of pluripotency. Nature cell biology. 2011; 13:490–496. [PubMed: 21540844]

Orkin SH, Hochedlinger K. Chromatin connections to pluripotency and cellular reprogramming. Cell. 2011; 145:835–850. [PubMed: 21663790]

Parker SC, Stitzel ML, Taylor DL, Orozco JM, Erdos MR, Akiyama JA, van Bueren KL, Chines PS, Narisu N, Program NCS, et al. Chromatin stretch enhancer states drive cell-specific gene regulation and harbor human disease risk variants. Proceedings of the National Academy of Sciences of the United States of America. 2013; 110:17921–17926. [PubMed: 24127591]

Pasini D, Bracken AP, Hansen JB, Capillo M, Helin K. The polycomb group protein Suz12 is required for embryonic stem cell differentiation. Mol Cell Biol. 2007; 27:3769–3779. [PubMed: 17339329]

Pasini D, Bracken AP, Jensen MR, Lazzerini Denchi E, Helin K. Suz12 is essential for mouse development and for EZH2 histone methyltransferase activity. The EMBO journal. 2004; 23:4061–4071. [PubMed: 15385962]

Pelish HE, Liau BB, Nitulescu II, Tangpeerachaikul A, Poss ZC, Da Silva DH, Caruso BT, Arefolov A, Fadeyi O, Christie AL, et al. Mediator kinase inhibition further activates super-enhancer-associated genes in AML. Nature. 2015; 526:273–276. [PubMed: 26416749]

Pokholok DK, Harbison CT, Levine S, Cole M, Hannett NM, Lee TI, Bell GW, Walker K, Rolfe PA, Herbolsheimer E, et al. Genome-wide map of nucleosorne acetylation and methylation in yeast. Cell. 2005; 122:517–527. [PubMed: 16122420]

Pulakanti K, Pinello L, Stelloh C, Blinka S, Allred J, Milanovich S, Kiblawi S, Peterson J, Wang A, Yuan GC, et al. Enhancer transcribed RNAs arise from hypomethylated, Tet-occupied genomic regions. Epigenetics. 2013; 8:1303–1320. [PubMed: 24135681]

Qian J, Wang Q, Dose M, Pruett N, Kieffer-Kwon KR, Resch W, Liang G, Tang Z, Mathe E, Benner C, et al. B cell super-enhancers and regulatory clusters recruit AID tumorigenic activity. Cell. 2014; 159:1524–1537. [PubMed: 25483777]

Quinlan AR, Hall IM. BEDTools: a flexible suite of utilities for comparing genomic features. Bioinformatics. 2010; 26:841–842. [PubMed: 20110278]

Rada-Iglesias A, Bajpai R, Swigut T, Brugmann SA, Flynn RA, Wysocka J. A unique chromatin signature uncovers early developmental enhancers in humans. Nature. 2011; 470:279–283. [PubMed: 21160473]

Rahl PB, Lin CY, Seila AC, Flynn RA, McCuine S, Burge CB, Sharp PA, Young RA. c-Myc regulates transcriptional pause release. Cell. 2010; 141:432–445. [PubMed: 20434984]

Rai AN, Vargas ML, Wang L, Andersen EF, Miller EL, Simon JA. Elements of the polycomb repressor SU(Z)12 needed for histone H3-K27 methylation, the interface with E(Z), and in vivo function. Mol Cell Biol. 2013; 33:4844–4856. [PubMed: 24100017]

Riising EM, Comet I, Leblanc B, Wu X, Johansen JV, Helin K. Gene silencing triggers polycomb repressive complex 2 recruitment to CpG islands genome wide. Molecular cell. 2014; 55:347–360. [PubMed: 24999238]

Sarma K, Margueron R, Ivanov A, Pirrotta V, Reinberg D. Ezh2 requires PHF1 to efficiently catalyze H3 lysine 27 trimethylation in vivo. Mol Cell Biol. 2008; 28:2718–2731. [PubMed: 18285464]

Schmitges FW, Prusty AB, Faty M, Stutzer A, Lingaraju GM, Aiwazian J, Sack R, Hess D, Li L, Zhou S, et al. Histone methylation by PRC2 is inhibited by active chromatin marks. Molecular cell. 2011; 42:330–341. [PubMed: 21549310]

Shen L, Shao N, Liu X, Nestler E. ngs.plot: Quick mining and visualization of next-generation sequencing data by integrating genomic databases. BMC Genomics. 2014; 15:284. [PubMed: 24735413]

Shen X, Liu Y, Hsu YJ, Fujiwara Y, Kim J, Mao X, Yuan GC, Orkin SH. EZH1 Mediates Methylation on Histone H3 Lysine 27 and Complements EZH2 in Maintaining Stem Cell Identity and Executing Pluripotency. Molecular cell. 2008; 32:491–502. [PubMed: 19026780]

Smith E, Lin C, Shilatifard A. The super elongation complex (SEC) and MLL in development and disease. Genes & development. 2011; 25:661–672. [PubMed: 21460034]

Strahl BD, Grant PA, Briggs SD, Sun ZW, Bone JR, Caldwell JA, Mollah S, Cook RG, Shabanowitz J, Hunt DF, et al. Set2 is a nucleosomal histone H3-selective methyltransferase that mediates transcriptional repression. Mol Cell Biol. 2002; 22:1298–1306. [PubMed: 11839797]

Strikoudis A, Lazaris C, Trimarchi T, Galvao Neto AL, Yang Y, Ntziachristos P, Rothbart S, Buckley S, Dolgalev I, Stadtfeld M, et al. Regulation of transcriptional elongation in pluripotency and cell differentiation by the PHD-finger protein Phf5a. Nature cell biology. 2016; 18:1127–1138. [PubMed: 27749823]

Subramanian A, Tamayo P, Mootha VK, Mukherjee S, Ebert BL, Gillette MA, Paulovich A, Pomeroy SL, Golub TR, Lander ES, et al. Gene set enrichment analysis: a knowledge-based approach for interpreting genome-wide expression profiles. Proceedings of the National Academy of Sciences of the United States of America. 2005; 102:15545–15550. [PubMed: 16199517]

Sun M, Lariviere L, Dengl S, Mayer A, Cramer P. A tandem SH2 domain in transcription elongation factor Spt6 binds the phosphorylated RNA polymerase II C-terminal repeat domain (CTD). The Journal of biological chemistry. 2010; 285:41597–41603. [PubMed: 20926372]

Trapnell C, Hendrickson DG, Sauvageau M, Goff L, Rinn JL, Pachter L. Differential analysis of gene regulation at transcript resolution with RNA-seq. Nature biotechnology. 2013; 31:46–53.

Vahedi G, Kanno Y, Furumoto Y, Jiang K, Parker SC, Erdos MR, Davis SR, Roychoudhuri R, Restifo NP, Gadina M, et al. Super-enhancers delineate disease-associated regulatory nodes in T cells. Nature. 2015; 520:558–562. [PubMed: 25686607]

Wang AH, Zare H, Mousavi K, Wang C, Moravec CE, Sirotkin HI, Ge K, Gutierrez-Cruz G, Sartorelli V. The histone chaperone Spt6 coordinates histone H3K27 demethylation and myogenesis. The EMBO journal. 2013; 32:1075–1086. [PubMed: 23503590]

Whyte WA, Orlando DA, Hnisz D, Abraham BJ, Lin CY, Kagey MH, Rahl PB, Lee TI, Young RA. Master transcription factors and mediator establish super-enhancers at key cell identity genes. Cell. 2013; 153:307–319. [PubMed: 23582322]

Wu H, Nord AS, Akiyama JA, Shoukry M, Afzal V, Rubin EM, Pennacchio LA, Visel A. Tissue-specific RNA expression marks distant-acting developmental enhancers. PLoS genetics. 2014; 10:e1004610. [PubMed: 25188404]

Yoh SM, Cho H, Pickle L, Evans RM, Jones KA. The Spt6 SH2 domain binds Ser2-P RNAPII to direct Iws1-dependent mRNA splicing and export. Genes & development. 2007; 21:160–174. [PubMed: 17234882]

Yoh SM, Lucas JS, Jones KA. The Iws1:Spt6:CTD complex controls cotranscriptional mRNA biosynthesis and HYPB/Setd2-mediated histone H3K36 methylation. Genes & development. 2008; 22:3422–3434. [PubMed: 19141475]

Young RA. Control of the embryonic stem cell state. Cell. 2011; 144:940–954. [PubMed: 21414485]

Zang C, Schones DE, Zeng C, Cui K, Zhao K, Peng W. A clustering approach for identification of enriched domains from histone modification ChIP-Seq data. Bioinformatics. 2009; 25:1952–1958. [PubMed: 19505939]

Zhang Y, Liu T, Meyer CA, Eeckhoute J, Johnson DS, Bernstein BE, Nussbaum C, Myers RM, Brown M, Li W, et al. Model-based analysis of ChIP-Seq (MACS). Genome biology. 2008; 9:R137. [PubMed: 18798982]

Zhu J, Adli M, Zou JY, Verstappen G, Coyne M, Zhang X, Durham T, Miri M, Deshpande V, De Jager PL, et al. Genome-wide chromatin state transitions associated with developmental and environmental cues. Cell. 2013a; 152:642–654. [PubMed: 23333102]

Zhu Y, Sun L, Chen Z, Whitaker JW, Wang T, Wang W. Predicting enhancer transcription and activity from chromatin modifications. Nucleic acids research. 2013b; 41:10032–10043. [PubMed: 24038352]

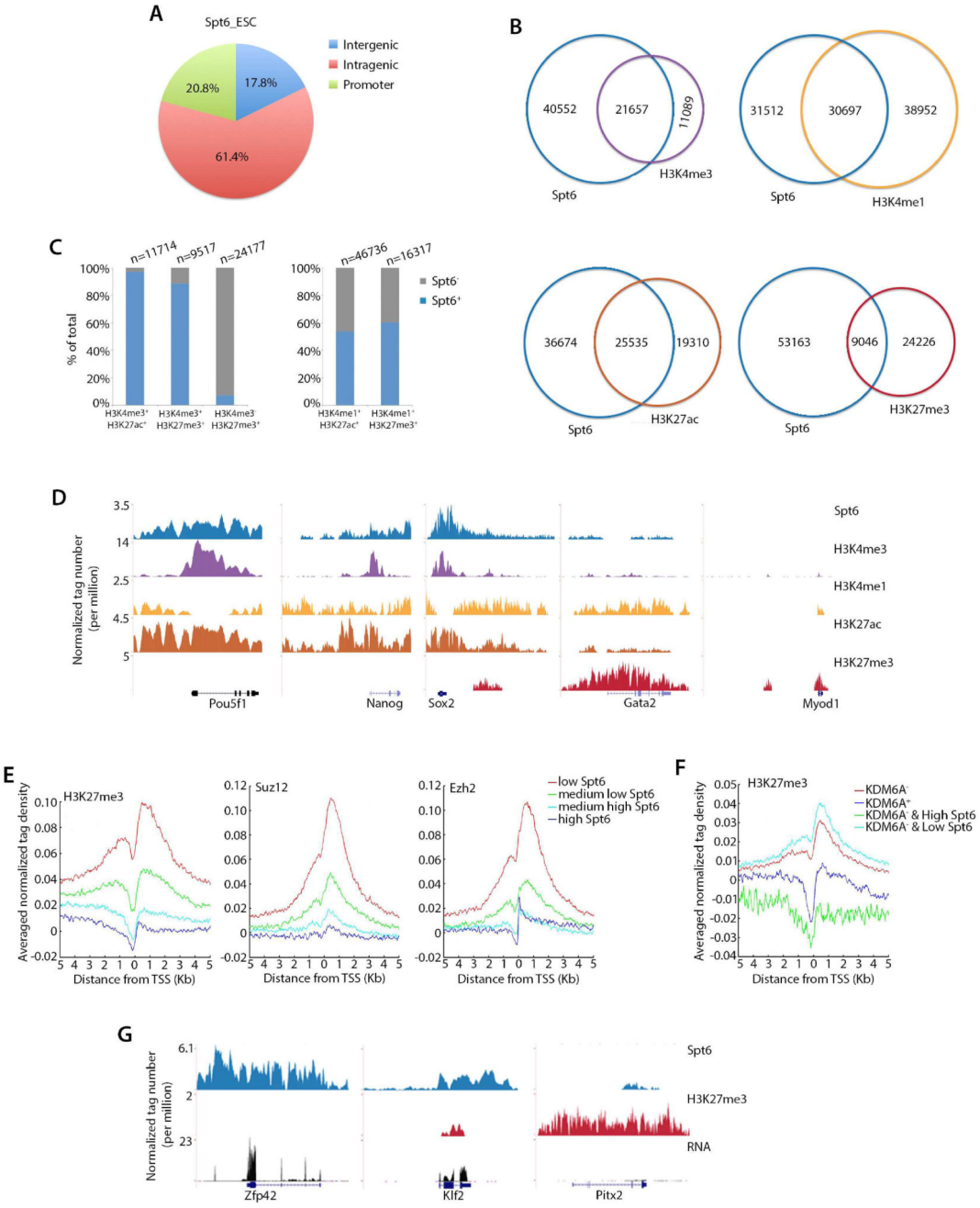

Figure 1. Genome-Wide Distribution of Spt6 in ESCs Negatively Correlates with PRC2 and H3K27me3

(A) Genome-wide distribution of Spt6 binding in ESCs. **(B)** Venn diagrams of genomic regions co-occupied by Spt6 and H3K4me3, H3K4me1, H3K27ac, or H3K27me3. **(C)** Bar graph depicting percentages of Spt6 peaks at TSS H3K4me3^{+}/H3K27ac^{+}, TSS H3K4me3^{+}/H3K27me3^{+}, H3K4me1^{+}/H3K27ac^{+}, H3K4me1^{+}/H3K27me3^{+}, and TSS (H3K4me3^{-}/H3K27me3^{+}). **(D)** Spt6, H3K4me3, H3K4me1, H3K27ac, and H3K27me3 ChIP-seq profiles at pluripotency genes (*Pou5f1, Nanog, Sox2*) and cell lineage-affiliated genes (*Gata2, Myod1*). **(E)** Averaged normalized tag densities of H3K27me3, Suz12, or Ezh2

ChIP-seq signals at regions with different Spt6 enrichment signal (low Spt6: lowest quartile; medium low and medium high Spt6: middle quartile; high Spt6; upper quartile) at transcriptional start sites (TSS). **(F)** Averaged normalized tag densities of H3K27me3 at KDM6A^{-}, KDM6A^{+}, KDM6A^{-}/high Spt6, or KDM6A^{-}/low Spt6 TSS. (**G**) Spt6 and H3K27me3 ChIP-seq and RNA-seq profiles at pluripotency genes (*Zfp42 and Klf2*) and cell lineage gene *Pitx2*.

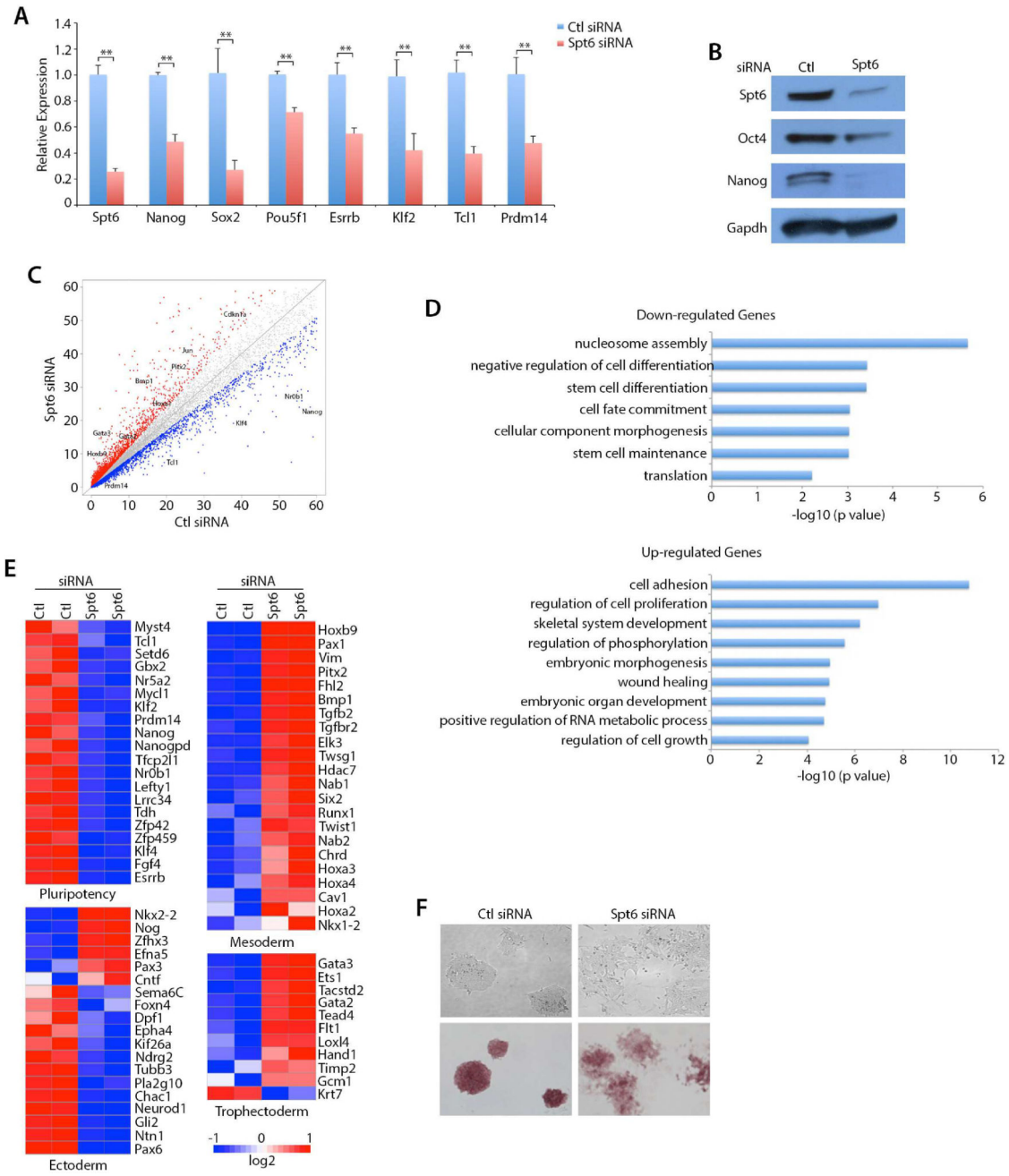

Figure 2. Spt6 Maintains Expression of Pluripotency Genes in ESC s

(A) Relative expression measured by qPCR of Nanog, Sox2, Pou5f1, Esrrb, Klf2, Tcl1, and Prdm14 transcripts from ESCs transfected with either control or Spt6 siRNA. Data are presented as mean ± SD (standard deviation) (n=3) (**) P<0.01. **(B)** ESCs were transfected with either control or Spt6 siRNA and cell extracts were immunoblotted with Spt6, Oct4, Nanog, and Gapdh antibodies. **(C)** Scatter plot of the RNA-Seq datasets from ESCs transfected with either control or Spt6 siRNA. Up- and down-regulated transcripts are in red and blue, respectively. **(D)** GO-biological processes associated with genes with ≥ 1.5-fold decreased (upper panel) or increased (lower panel) expression from ESCs transfected with

either control or Spt6 siRNA. **(E)** Heatmaps representing the $\log_2$ expression values for genes associated with pluripotency, mesoderm, ectoderm, and trophoectoderm obtained by RNA-Seq of ESCs transfected with either control or Spt6 siRNA. **(F)** Phase contrast microscopy of ESCs transfected with either control or Spt6 siRNA (top panel), and immunohistochemistry staining with the pluripotency marker alkaline phosphatase (AP) (lower panel).

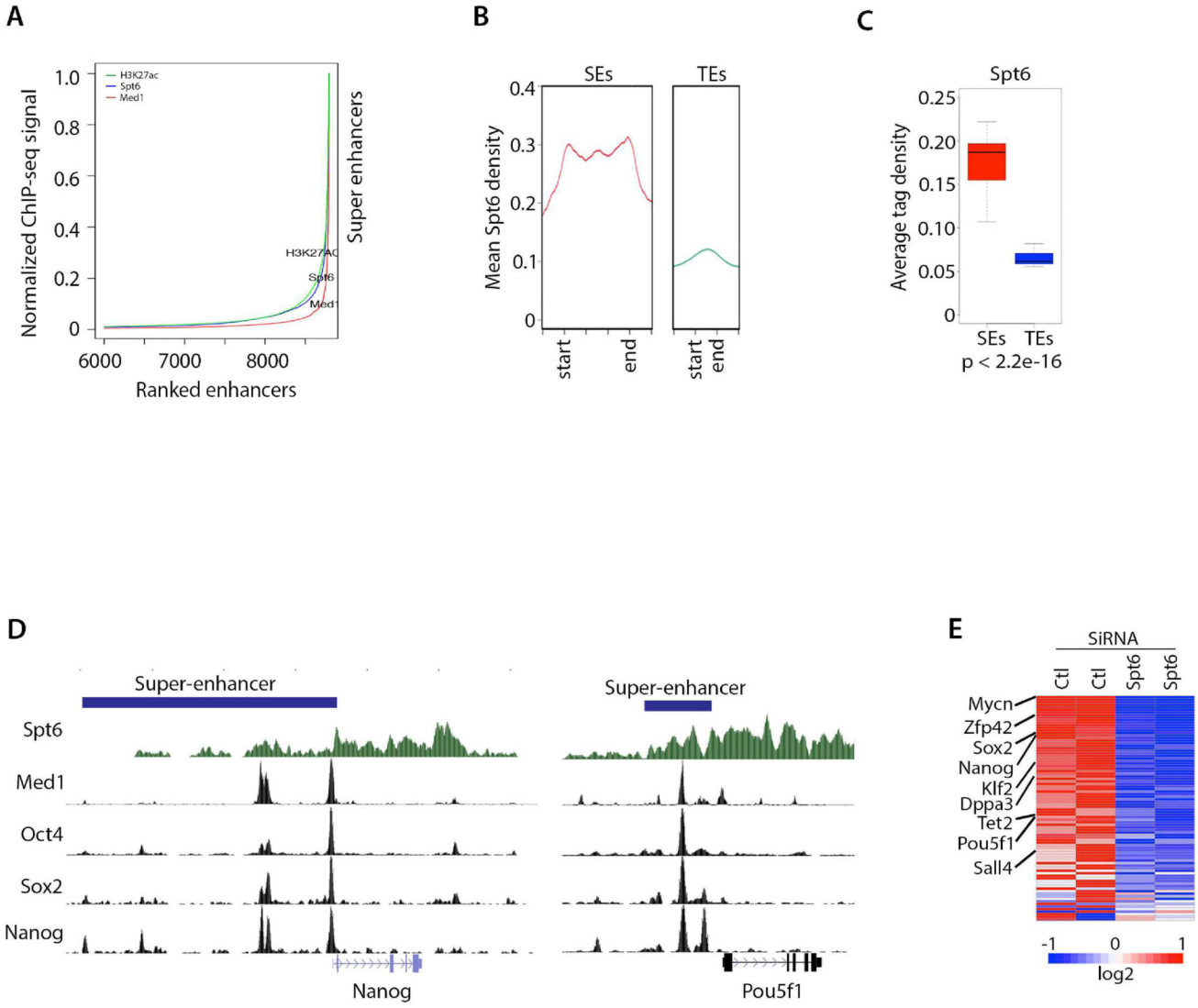

Figure 3. Spt6 is Enriched at ESC Super-Enhancers

(A) Distribution of Med1, H3K27ac, and Spt6 normalized ChIP-seq signals across a subset of 8,794 ESC enhancers. Med1, H3K27ac, and Spt6 are enriched at a subset of enhancers (super-enhancers). **(B)** Metagenes of Spt6 ChIP-seq density (reads per million reads per base pair) across the 231 super-enhancers (SE) and the 8,563 typical enhancers (TE). **(C)** Box plot of Spt6 ChIP-seq density at SE and TE regions. **(D)** Spt6, Med1, Oct4, Sox2, and Nanog occupancies for super-enhancer regions of *Nanog* and *Pou5f1* (*Oct4*) loci. **(E)** Heatmap representing the $\log_2$ expression values of SE-associated genes in ESCs transfected with either control or Spt6 siRNA.

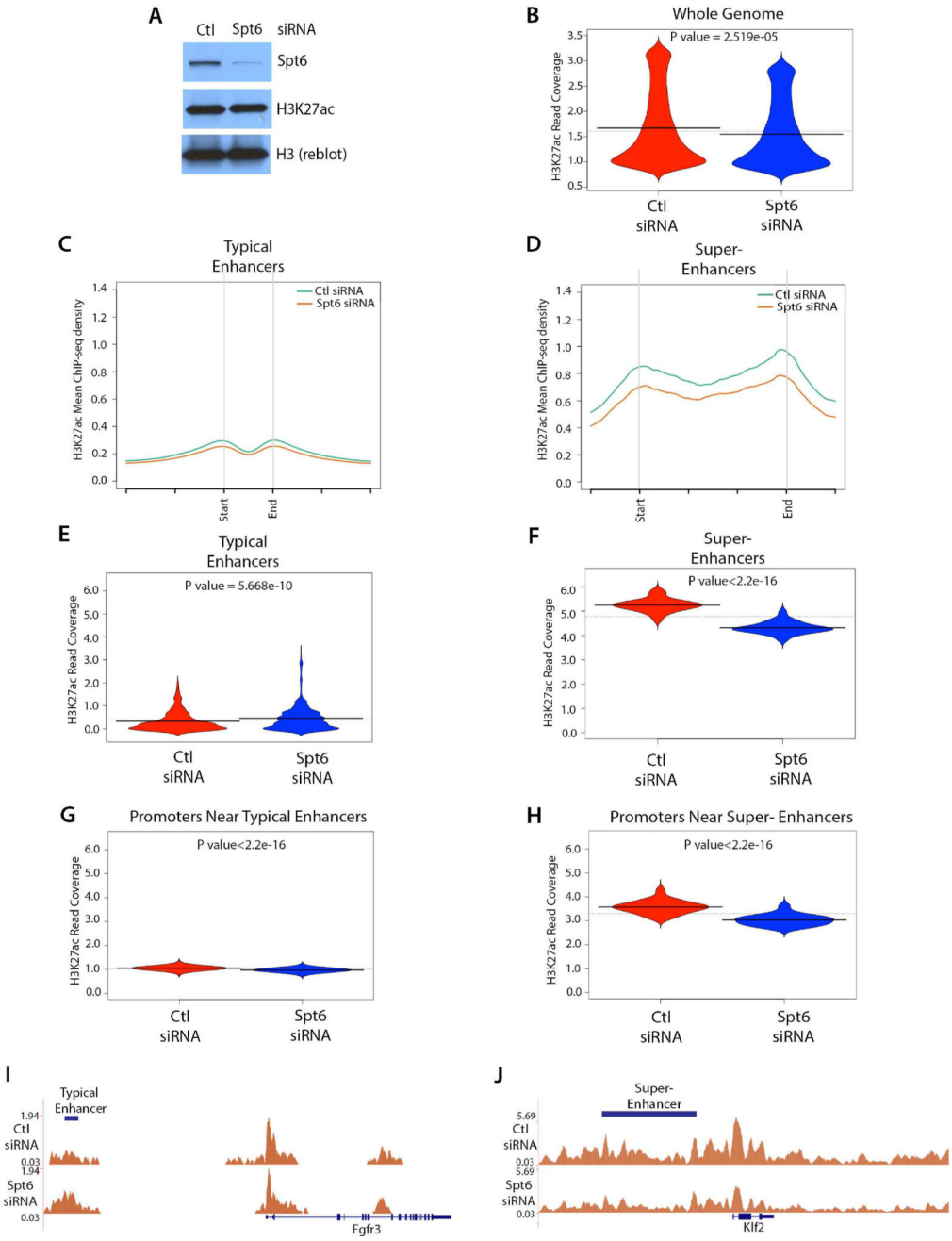

Figure 4. H3K27ac is Reduced at Super-Enhancers and Associated Promoters of Spt6-Depleted ESCs

(A) Cell extracts of control or Spt6 siRNA ESCs were immunoblotted with Spt6, H3K27ac, and unmodified histone H3 antibodies. **(B)** Genome-wide H3K27ac coverage in control and Spt6 siRNA ESCs. **(C)** Average ChIP-seq read density of H3K27ac at typical enhancers in control and Spt6 siRNA ESCs. **(D)** Average ChIP-seq read density of H3K27ac at super-enhancers in control and Spt6 siRNA ESCs. **(E)** Violin plots representing H3K27ac read coverage at typical enhancers in control and Spt6 siRNA ESCs. **(F)** Violin plots representing H3K27ac read coverage at super-enhancers in control and Spt6 siRNA ESCs. **(G)** Violin

plots representing H3K27ac read coverage at promoters associated with typical enhancers in control and Spt6 siRNA ESCs. **(H)** Violin plots representing H3K27ac read coverage at promoters associated with super-enhancers in control and Spt6 siRNA ESCs. **(I)** H3K27ac ChIP-seq profiles at the *Fgfr3* locus in control and Spt6 siRNA ESCs. **(J)** H3K27ac ChIP-seq profiles at the *Klf2* locus in control and Spt6 siRNA ESCs.

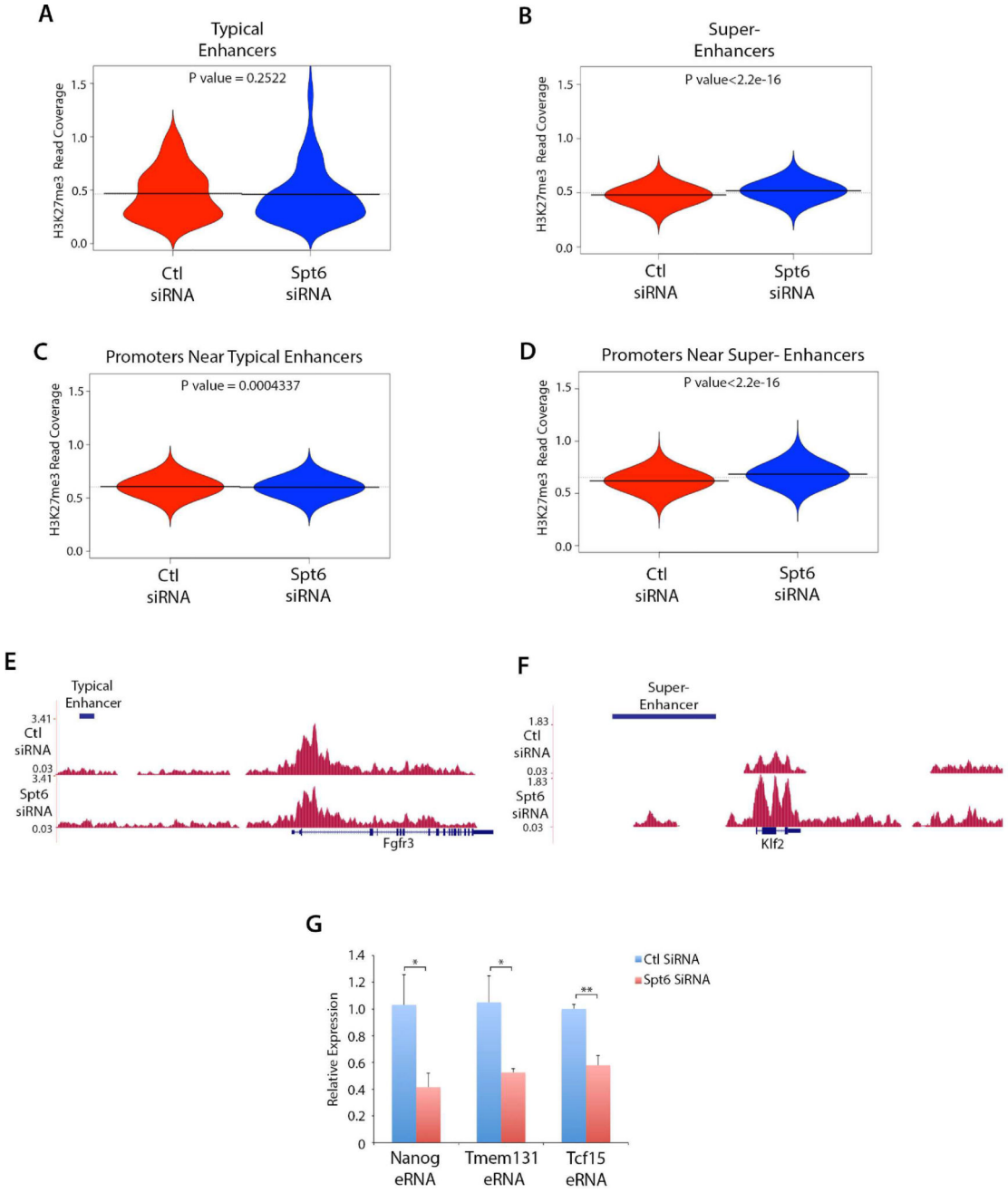

Figure 5. H3K27me3 is Increased at Super-Enhancers and Associated Promoters of Spt6-Depleted ESCs

(A) Violin plots representing H3K27me3 read coverage at typical enhancers in control and Spt6 siRNA ESCs. **(B)** Violin plots representing H3K27me3 read coverage at super-enhancers in control and Spt6 siRNA ESCs. **(C)** Violin plots representing H3K27me3 read coverage at promoters associated with typical enhancers in control and Spt6 siRNA ESCs. **(D)** Violin plots representing H3K27me3 read coverage at promoters associated with super-enhancers in control and Spt6 siRNA ESCs. **(E)** H3K27me3 ChIP-seq profiles at the *Fgfr3* locus in control and Spt6 siRNA ESCs. **(F)** H3K27ac ChIP-seq profiles at the *Klf2* locus in

control and Spt6 siRNA ESCs. **(G)** RT-qPCR for Nanog, Tmem 131, and Pcf15 enhancer RNA transcripts in ESCs transfected with either control or Spt6 siRNA. Data are presented as mean ± SD (n=3) (*) $P < 0.05$, (**) $P < 0.01$.

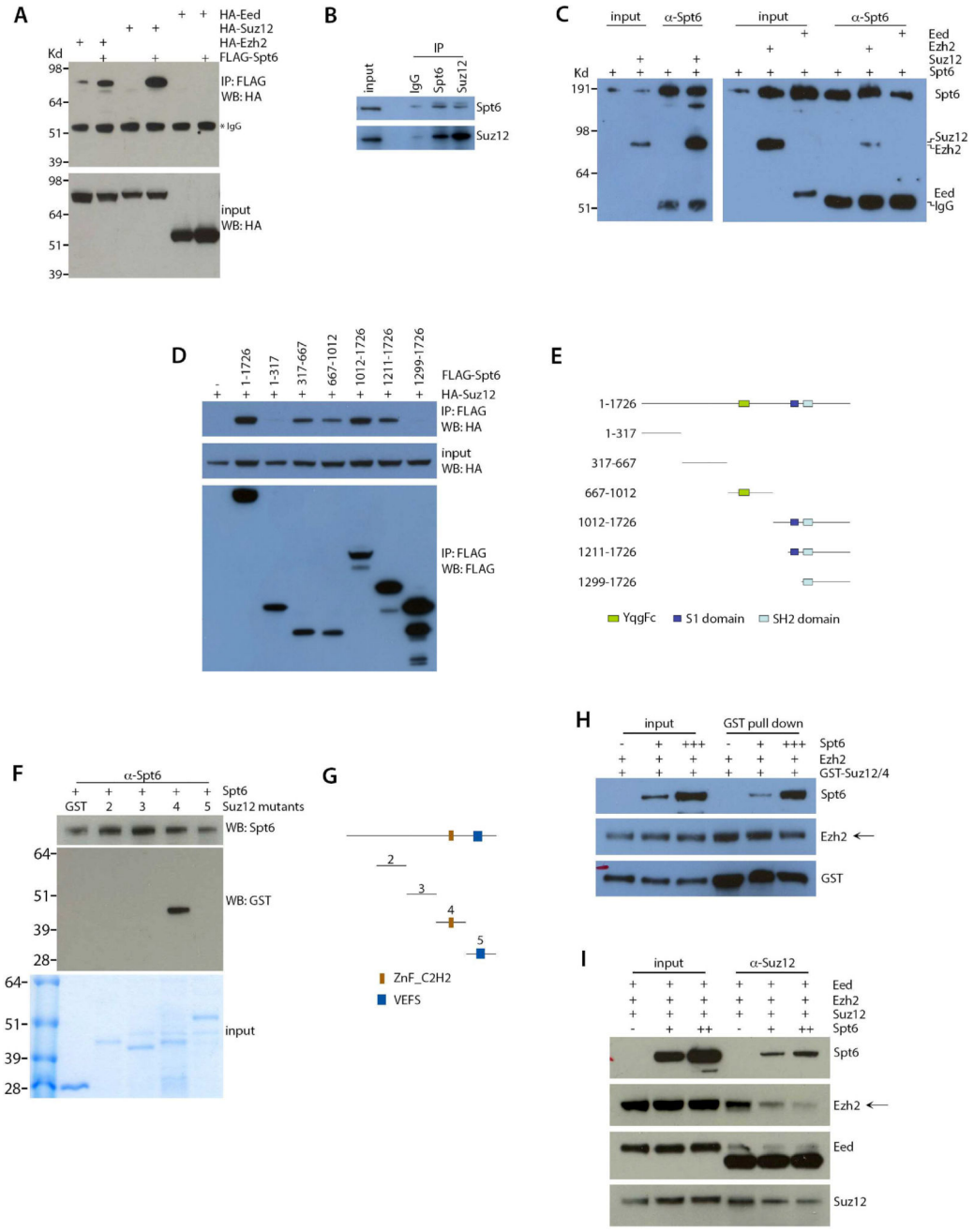

Figure 6. Spt6 Directly Interacts with Suz12 and Competes for Ezh2 binding

(A) FLAG-Spt6 and HA-Ezh2, HA-Suz12 and HA-Eed constructs were transfected in 293T cells. Extracts from transfected cells were immunoprecipitated with FLAG resin (M2) and immunoblotted with either HA or FLAG antibodies. IgG indicates a band corresponding to immunoglobulin heavy chains. **(B)** ESC nuclear extracts were immunoprecipitated with IgG, Spt6 or Suz12 and immunoblotted with Spt6 or Suz12 antibodies. **(C)** Baculovirus–expressed Spt6, Ezh2, Suz12 and Eed proteins were incubated and immunoprecipitated with a Spt6 antibody. Immunocomplexes were subjected to immunoblotting with Spt6, Ezh2, Eed or Suz12 antibodies. IgG indicates a band corresponding to immunoglobulin heavy chains.

(D) FLAG-tagged Spt6 full-length (amino acids 1–1726) and deletion mutants and HA-Suz12 constructs were transfected in 293T cells. Extracts from transfected cells were immunoprecipitated with FLAG resin (M2) and immunoblotted with either HA or FLAG antibodies. **(E)** Schematic representation of Spt6 constructs transfected in experiments described in **(D)**. YqgFc indicates a potential resolvase/ribonuclease domain; S1 an RNA-binding domain; and SH2 a Src-Homology 2 domain (Sun et al., 2010). **(F)** Baculovirus-expressed and purified Spt6 protein and bacterially-expressed and purified GST-Suz12 polypeptides were incubated and immunoprecipitated with a Spt6 antibody. Immunocomplexes were subjected to immunoblotting with either Spt6 or GST antibodies (top panel). Coomassie staining of input GST control and GST-Suz12 polypeptides (lower panel). **(G)** Schematic representation of the GST-Suz12 constructs employed in experiments described in (**F**). VEFS indicate a Vrn2-Emf2-Fis2-Su(z)12 domain and ZnF_CH2 a zinc finger domain (Birve et al., 2001). **(H)** GST-Suz12 (amino acids 406–545) (corresponding to construct 4 in **G**), Ezh2 and different amounts of Spt6 proteins were incubated and processed for GST pull-down assay. The beads-bound complexes were subjected to immunoblotting with Spt6, Ezh2 or GST antibodies. Decreasing amounts of Ezh2 (arrow) are retrieved by Suz12 immunoprecipitation in the presence of increasing amounts of Spt6. **(I)** Cell extracts from 293T cells transfected with Ezh2, Eed, Suz12 and different amounts of Spt6 expression vectors were incubated and immunoprecipitated with a Suz12 antibody. Immunocomplexes were subjected to immunoblotting with Spt6, Ezh2, Eed and Suz12 antibodies. Decreasing amounts of Ezh2 (arrow) are retrieved by Suz12 immunoprecipitation in the presence of increasing amounts of Spt6.

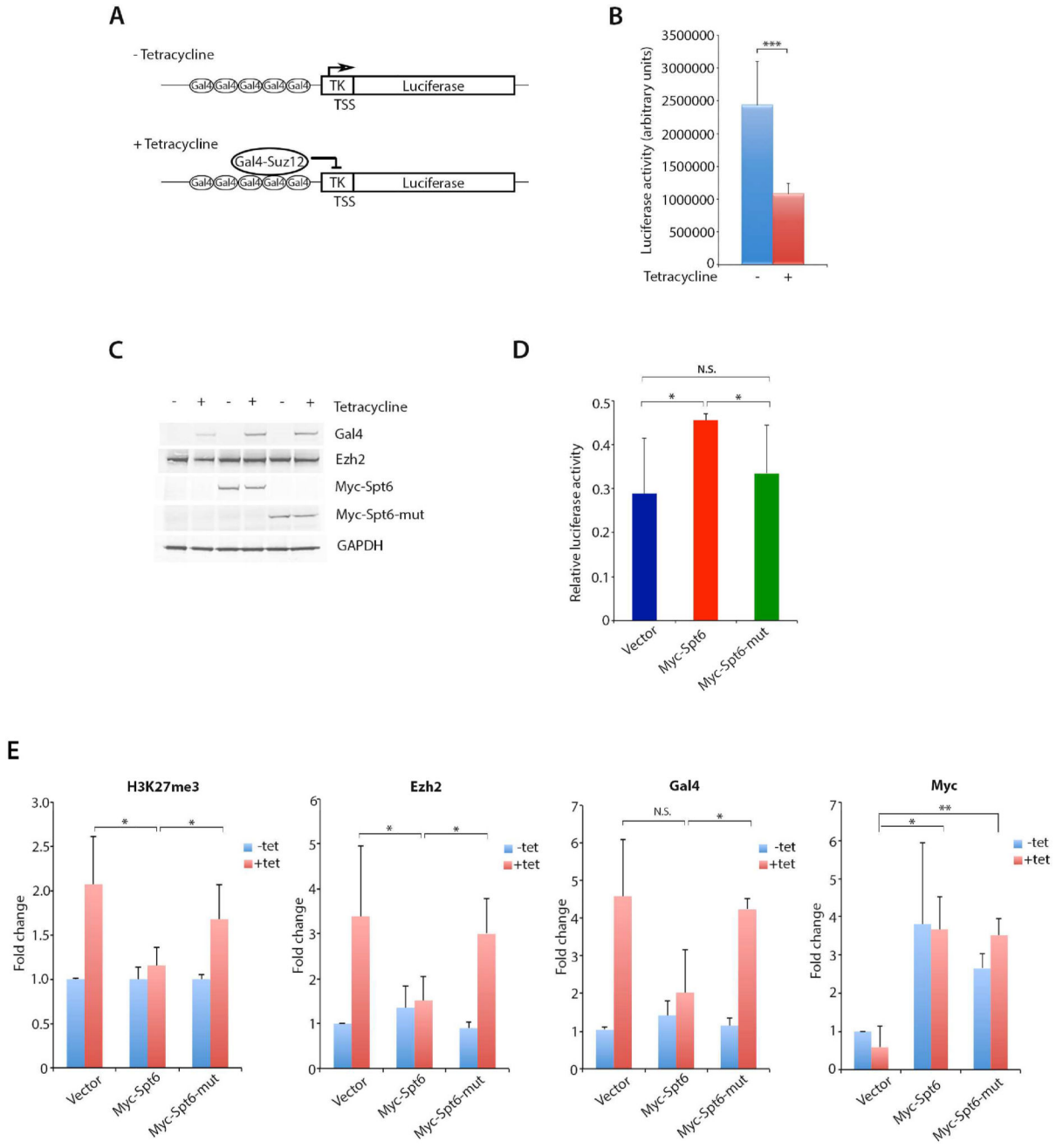

Figure 7. Spt6 Counteracts PRC2 Chromatin Recruitment and Transcriptional Repression

(A) Schematic representation of the 293 Gal4-Suz12/Gal4-TK-Luc reporter system. **(B)** Luciferase activity in 293 cells stably transfected with Gal4-TK-luciferase reporter and tetracycline-regulated Gal4-Suz12 expression vector. The values of luciferase activity are the mean ± SD (standard deviation) of three independent biological replicates. (***) P<0.005. **(C)** Cell extracts from 293 Gal4-Suz12/Gal4-TK-Luc cells grown in the absence (−) or presence (+) of tetracycline for 24h after being transfected with control, full length or C-terminal amino acids 1299–1726 Myc-tagged Spt6 vectors were immunoblotted with Gal4, Ezh2, Myc, and GAPDH antibodies.

(D) Luciferase activity in 293 Gal4-Suz12/Gal4TK-Luc cells transiently transfected with control (vector), full length or C-terminal amino acids 1299–1726 Myc-tagged Spt6 vectors. The values of luciferase activity are the mean ± SD (n=3). (*) P<0.05 when compared control and Spt6 vectors with tetracycline induction. N.S., not statistically significant. **(E)** 293 Gal4-Suz12/Gal4TK-Luc cells grown in the absence (−) or presence (+) of tetracycline were transfected with control, full length or C-terminal amino acids 1299–1726 Myc-tagged Spt6 vectors and processed for ChIP assay using the indicated antibodies. The immunoprecipitated DNA was quantified by qPCR. Data are presented as mean ± SD (n=3) (*) $P < 0.05$, (**) $P < 0.01$.

KEY RESOURCES TABLE

REAGENT or RESOURCE	SOURCE	IDENTIFIER
Antibodies		
Rabbit polyclonal anti-Spt6	Novus	NB100-2582
Rabbit monoclonal anti-Suz12 (D39F6)	Cell Signaling Technology	#3737
Rabbit monoclonal anti-Ezh2 (D2C9)	Cell Signaling Technology	#5246
Mouse monoclonal anti-Ezh2 (AC22)	Cell Signaling Technology	#3147
Rabbit polyclonal anti-Eed	EMD Millipore	09-774
Rabbit polyclonal anti-KDMA6A	Sigma	HP A000568
Rabbit polyclonal anti-H3K27me3	EMD Millipore	07-449
Rabbit monoclonal anti-H3K27me3 (C36B11)	Cell Signaling Technology	9733
Rabbit polyclonal anti-H3K27ac	Abcam	ab4729
Rabbit polyclonal anti-H3K36me3	Abcam	ab9050
Rabbit Polyclonal anti-H3	Abcam	ab1791
Rabbit Polyclonal anti-Oct4 (Pou5f1)	Abcam	Ab19857
Rabbit Polyclonal anti-Nanog	Cosmo Bio	RCAB0002P–F
Rabbit monoclonal anti-Gapdh	Cell Signaling Technology	2118
Mouse monoclonal anti-RNA polymerase II phospho S2 (H5)	Abcam	ab24758
Rabbit polyclonal anti-Gal4	EMD Millipore	06-262
Mouse monoclonal anti-FLAG (M2)	Sigma	F3165
Mouse monoclonal anti-Myc	Sigma	M4439
Rabbit anti-HA (Y-11)	Santa Cruz	sc-805
Rabbit polyclonal anti-GST	Santa Cruz	sc-459
Mouse monoclonal anti-GST	Santa Cruz	sc-138
Rabbit IgG	Abcam	ab171870
Mouse IgG	Abcam	ab37355
Anti-FLAG M2 Affinity Gel	Sigma	A2220
Glutathione Sepharose 4B	GE Healthcare	17075601
Protein A-Agarose	Roche	11134515001
Protein G-Agarose	Roche	11719416001
HisPur Ni-NTA Resin	Thermo Fisher Scientific	88221
HisPur Cobalt Resin	Thermo Fisher Scientific	89964
Dynabeads Protein G	Thermo Fisher Scientific	10004D
Bacterial and Virus Strains		
DH5α competent cells	Thermo Fisher Scientific	18265017
One Shot Stbl3 Chemically competent *E.coli*	Thermo Fisher Scientific	C737303
One Shot BL21 Star (DE3) Chemically competent *E.coli*	Thermo Fisher Scientific	C601003

REAGENT or RESOURCE	SOURCE	IDENTIFIER
DH10Bac Competent Cells	Thermo Fisher Scientific	10361012
Sf9 Insect Cells - Novagen	EMD Millipore	71104
Chemicals, Peptides, and Recombinant Proteins		
ESGRO Leukaemia inhibitory factor [LIF]	EMD Millipore	ESG1107
Lipofectamine 2000 Transfection Reagent	Thermo Fisher Scientific	11668-019
Lipofectamine RNAiMAX Reagent	Thermo Fisher Scientific	13778-150
TRIzol Reagent	Thermo Fisher Scientific	15596018
Blasticidin	Thermo Fisher Scientific	A1113903
Zeocin	Thermo Fisher Scientific	R25001
G418	Thermo Fisher Scientific	11811-031
Tetracycline hydrochloride	Sigma	T7660
EmbryoMax 0.1% Gelatin Solution	EMD Millipore	ES-006-B
Protease Inhibitor	Roche	11836170001
Mouse His-Spt6	This paper	N/A
Human FLAG-Ezh2	This paper	N/A
Human His-Suz12	This paper	N/A
Human His-Eed	This paper	N/A
Human GST-Suz12 (151–294)	This paper	N/A
Human GST-Suz12 (293–405)	This paper	N/A
Human GST-Suz12 (406–542)	This paper	N/A
Human GST-Suz12 (542–740)	This paper	N/A
Critical Commercial Assays		
Alkaline Phosphatase Detection Kit	EMD Millipore	SCR004
High Capacity cDNA Reverse Transcription Kit	Thermo Fisher Scientific	4368814
Power SYBR Green PCR Master Mix	Thermo Fisher Scientific	4368708
Dual-Luciferase Reporter Assay System	Promega	E1910
Deposited Data		
ChIP and RNA-seq data GSE103180	This paper	N/A
Raw data	This paper	doi:10.17632/2z6749m9xs.1
Experimental Models: Cell Lines		
ES E14TG2a	ATCC	CRL-1821
HEK 293T cells	ATCC	CRL-1573
CF-1 MEF feeder, irradiated	MTI-GlobalStem	GSC-6001G
Mouse embryonic fibroblasts (MEF)	ATCC	SCRC-1040
293T rex with 5xGal4RE-tk-lcG2a	Dr. Danny Reinberg	Sarma, et al. 2008
293T rex with 5xGal4RT-tk-luc and Gal4-Suz12	This paper	N/A
Oligonucleotides		
siRNA: Mm_Supt6h_4 sense: AGAAGUUUCUUGUGAAUAATT	Qiagen	SI01438080

REAGENT or RESOURCE	SOURCE	IDENTIFIER
siRNA: Mm_Supt6h_4 antisense: UUAUUCACAAGAAACUUCUTT	Qiagen	SI01438080
AllStars Negative Control siRNA	Qiagen	SI03650318
Recombinant DNA		
pCMV-Tag2B vector	Agilent	N/A
pCMV-Tag2B–Spt6 wt and various mutants	This paper	N/A
pCMVHA hEzh2	Addgene	#24230
pCMVHA Suz12	Addgene	#24232
pCMVHA EED	Addgene	#24231
pcDNA5-FRT-TO	Thermo Fisher Scientific	N/A
pcDNA5/FRT/TO-Gal4-Suz12	This paper	N/A
pGEX-4t-1	GE Healthcare	N/A
pGEX-4t-1-Suz12 mutant 2 (151–294)	This paper	N/A
pGEX-4t-1-Suz12 mutant 3 (293–405)	This paper	N/A
pGEX-4t-1-Suz12 mutant 4 (406–542)	This paper	N/A
pGEX-4t-1-Suz12 mutant 5 (542–740)	This paper	N/A
pFastBac HT-A	Thermo Fisher Scientific	N/A
pFastBac HT-A-Spt6	This paper	N/A
pFastBac-His-FLAG-Ezh2	Dr. Danny Reinberg	N/A
pAcHLT-His-Suz12	Dr. Danny Reinberg	N/A
pAcHLT-His-Eed	Dr. Danny Reinberg	N/A
Software and Algorithms		
CASAVA	Illumina	https://support.illumina.com/downloads/casava_18_changes.html
Bowtie	Langmead et al., 2009	http://bowtie-bio.sourceforge.net/bowtie2/index.shtml
SICER	Zang et al., 2009	http://home.gwu.edu/~wpeng/Software.htm
Bedtools	Quinlan and Hall, 2010	http://bedtools.readthedocs.io/en/latest/
Homer	Heinz et al., 2010	http://homer.ucsd.edu/homer/
MACS2	Zhang et al., 2008	https://github.com/taoliu/MACS
Tophat2	Kim et al., 2013	https://ccb.jhu.edu/software/tophat/index.shtml
Cufflinks/Cuffdiff	Trapnell et al., 2013	http://cole-trapnell-lab.github.io/cufflinks/cuffdiff/
GSEA	Broadinstitute	http://www.broadinstitute.org/gsea